Diurnal stomatal apertures and density ratios affect whole-canopy stomatal conductance, water-use efficiency and yield

Sanbon Chaka Gosa[1], Bogale Abebe Gebeyo[12], Ravitejas Patil[1], Ramón Mencia [1] Menachem Moshelion[1#]

[1] The R.H. Smith Institute of Plant Sciences and Genetics in Agriculture, The R.H. Smith Faculty of Agriculture, Food and Environment, The Hebrew University of Jerusalem, Rehovot, 76100 Israel

[2] Current address: Department of Horticulture, College of Agriculture and Natural Resource, Dilla University, Dilla, Ethiopia

#Corresponding Author, (menachem.moshelion@mail.huji.ac.il)

Short Running Head: Dynamic stomatal and whole-plant responses

Plant dynamic responses from stomata to whole plant

Abstract

Key physiological traits of plants, such as transpiration and stomatal conductance, are usually studied under steady-state conditions or modeled using only a few measured data points. Those measurements do not reflect the dynamic behavior of the plant in response to field conditions. To overcome this bottleneck, we used a gravimetric functional-phenotyping platform and a reverse-phenotyping method to examine the dynamic whole-plant water-regulation responses of tomato introgression lines and compared those responses with several years of yield performance in commercial fields. Ideotype lines had highly plastic stomatal conductance and high abaxial–adaxial stomatal density ratios and the size of their stomatal apertures peaked early in the day under water-deficit conditions. These traits resulted in dynamic daily water-use

efficiency, which allowed for the rapid recovery of transpiration when irrigation was resumed after a period of imposed drought. We found that stomatal density, the abaxial–adaxial stomatal density ratio and the time of maximum stomatal apertures are crucial for plant adaptation and productivity under drought-stress conditions. Abaxial stomatal density was also found to be strongly correlated with the expression of the stomatal-development genes *SPCH* and *ZEP*. This study demonstrates how a reverse functional phenotyping approach based on field yield data, continuous and simultaneous whole-plant water-balance measurements and anatomical examination of individual leaves can help us to understand and identify dynamic and complex yield-related physiological traits.

Keywords: functional phenotyping, crops yield, dynamic response, drought stress, stomatal conductance, reverse phenomics

Introduction

Agricultural crop productivity must increase significantly to meet the food needs of the world's growing population (FAO, 2017). The need to increase yields, in general, and under stressful conditions, in particular, while reducing damage to the environment continues to be a very important challenge (Tian et al., 2021). The most promising strategy for meeting this challenge is to improve crop genetics through breeding, based on an understanding of genomics and the ability to correctly phenotype plants and their environmental interactions (i.e., genotype–environment interactions or G×E) [Furbank and Tester (2011), as reviewed in (Gao, 2021)]. The less accurate quantification of plant traits related to stress has hindered the translation of genomic data into valued phenotypes (Mir et al., 2019). Therefore, the bottleneck in exploiting crop traits for high productivity under stress is shifting from high-throughput genomics to high-throughput phenomics capable of predicting yield and resilience in the field.

The first decade of the phenomic era has seen remarkable advances in phenotyping platforms. Nonetheless, the impacts are still far from satisfactory, mainly due to plants' extremely plastic phenotypic responses to their environments (Duursma et al., 2019). In fact, due to their sessile lifestyle (Claeys and Inzé, 2013), plants are the most plastic macro-organisms on earth (Schlichting, 1986), exhibiting dramatic phenotypic and physiological plasticity in response to environmental conditions (Moshelion, 2020). Even under controlled laboratory conditions, significant variations have been observed in leaf growth and other traits of Arabidopsis WT col 0 across 10 laboratories, due to differences in the environmental conditions (Massonnet et al., 2010).

In response to complex and uncertain environmental conditions, plants exhibit plastic behavior to optimize their water-use efficiency (WUE) at any given moment

(Hetherington and Woodward, 2003). This plastic behavior poses some challenges to a classical gene-to-trait research approach, as the relationship between the genotype and the observed traits will vary with the prevailing environmental conditions (Wardle, 2013). In fact, it is rather challenging to establish a gene or QTL that contributes to yield, in general, and drought responses, in particular, due to the complexity and quantitative nature of yield-related traits. This process takes a very long time (Sandhu et al., 2021), which limits the number of promising candidates that reach the field-experiment stage (Moshelion and Altman, 2015). To deal with these challenges, pre-field functional screening of candidate genotypes is expected to dramatically reduce the amount of effort required for breeding for resistance to abiotic stress (Negin and Moshelion, 2017). These screening processes should be relatively short, simulate field conditions, consider the spatial and temporal G×E and be replicable.

Determining yield-related traits, particularly at an early growth stage, is one of the biggest challenges in pre-breeding programs (Voss-Fels et al., 2019). The rate of photosynthesis directly reflects plant productivity. Therefore, the rate of photosynthesis would be a good parameter to use to predict yield-related traits, in order to select the best candidates at an early growth stage (Sallam et al., 2019). Nevertheless, to date, no reliable high-throughput tool exists for measuring the whole-plant photosynthetic rate continuously and simultaneously across numerous plants and under dynamic ambient conditions. As plant water-balance regulation mechanisms optimize productivity–vulnerability trade-offs through the regulation of stomatal aperture (Shahinnia et al., 2016), the measurement of stomatal conductance (g_s) and transpiration could serve as another good screening strategy. These key traits are frequently studied using steady-state measurements that do not reflect plant behavior under dynamic field conditions (Chazdon and Pearcy, 1986), 1986; (Matthews et al., 2017).

Levels of g_s and transpiration are determined by several anatomical-morphological traits such as stomatal density, size, aperture and distribution, as well as leaf shape and boundary layers (Ohsumi et al., 2007; Shahinnia et al., 2016), which are challenging to phenotype. A recent work by (Vialet-Chabrand et al., 2013, (Durand et al., 2019) demonstrated that dynamic models predict g_s more accurately than steady-state models. In addition, continuous measurement of these traits in whole young tomato plants revealed that they are closely related to yield performance in the field (Gosa et al., 2022).

The actual dynamics of whole-canopy conductance (Gsc) and its interactions with the environment are still poorly understood. This underscores the importance of accurate physiological phenotyping for improved crop breeding (Ghanem et al., 2015). Whole-plant G×E functional phenotyping platforms are an important tool for meeting the challenges of the phenomic era (Dalal et al., 2020). These platforms provide valid and reliable data regarding the stomatal behavior of the whole plant (Roman et al., 2021). The stomatal-aperture response is affected by both external ambient conditions and the plant's internal biochemical-physiological state. We hypothesized that the speed of the stomatal response to momentary changes in ambient conditions plays a key role in the optimization of the whole-plant momentary WUE, to maximize plant yield under the dynamic and uncertain conditions present throughout the growing season.

In this study, we used reverse phenotyping for a multiple-year field experiment, in which the yields and plant weights of tomato introgression lines (IL) were monitored under both wet and dry conditions. This allowed us to identify 29 IL lines with a spectrum of key traits varying from high yield, high resilience and high tolerance (idiotype) to low-yield, low-tolerance and low-resilience lines. The key physiological

traits of the superior-performing and poor-performing lines at a very early growth stage were phenotyped using manual measurements of leaf gas exchange, stomatal imprinting and an automated functional-phenotyping platform. We demonstrated the benefits of continuous and simultaneous tracking of whole-plant water-balance regulation traits in response to fluctuating environmental conditions, as opposed to single time-point measurements. In this manner, were able to link the leaf-level data with whole-plant physiological data measured in a greenhouse and open-field yield data, to study the traits of high-yielding genotypes under well-irrigated and drought stress conditions.

Materials and Methods

Field experiments

In this study, we used a total of 30 tomato genotypes: 29 ILs derived from crossings of *Solanum pennellii* and the cultivar M82 (*Solanum lycopersicum* cv. M82; Table 1). Each of the lines contained a single homozygous restriction fragment-length polymorphism of *Solanum pennellii* chromosome segment (Eshed and Zamir, 1995). For the genotype-performance screening of seven selected genotypes, we used historical yield data from several field experiments performed in 1993, 2000, 2001, 2002, 2003, 2004 and 2010. In brief, the open-field experiments were performed at the Western Galilee Experimental Station, in Akko, Israel, during the summer in a randomized block design, as described in (Gur and Zamir, 2004). Those trials involved a planting density of one plant per m^2. Both wet and dry fields started during the growing season at field water capacity. There was no rain during the experimental period, so the irrigation system alone was used to manage the drought scenarios. Details

of the agricultural practices and measurements have been published previously (Fridman et al., 2000; Gur and Zamir, 2004)

Leaf gas-exchange measurements

Plants were grown in the ground (sandy-loam soil) in a semi-controlled greenhouse at the Hebrew University of Jerusalem, Faculty of Agriculture in Rehovot, Israel. The genotypes were planted and measured in random order. We measured leaf gas-exchange on the youngest, fully extended leaf. Measurement data were collected from mature, fully expanded leaflets at the top of the canopy of ~8-week-old plants between 10:00 am and 12:00 am. A portable infra-red gas analyzer (LI-6800XT; Li-Cor Inc., Lincoln, NE, USA) was used to obtain the carbon assimilation rate (A_N). Stomatal conductance (g_s) was measured in a 6-cm^2 chamber, at midday, with the CO_2 reference set at 400 mmol m^{-2} s^{-1}, PAR at 400 mmol m^{-2} s^{-1}, VPD at 1.4 kPa and temperature set at 25°C. Those levels were chosen to mimic the environmental conditions in the greenhouse at the time of the initial measurements.

Reverse phenomics using the physiological-phenotyping platform in a greenhouse

Using the functional telemetric platform comprised of weighing lysimeters, soil and atmosphere sensors (Plantarray, PA 3.0, PlantDitech Ltd., Yavne, Israel), we continuously monitored plant growth and water balance through controlled tracking and measurement of the transpiration and biomass gain of each plant throughout the growing period. At the same time, we also monitored the soil and atmospheric conditions around the plants (see Fig. 1), as described in (Dalal et al., 2020).

Experimental setup

Five-week-old seedlings of eight selected ILs and M82 tomato plants were transplanted into pots and grown in a greenhouse belonging to the Israeli Center of Research

Excellence (ICORE) for Plant Adaptation to the Changing Environment, at The Hebrew University of Jerusalem, Faculty of Agriculture in Rehovot, Israel, during September 2019. An overview of the nutrients supplied to the plants via the irrigation system (fertigation) is presented in (Dalal et al., 2020). Before the start of the experiment, all load-cell units were calibrated for accuracy and drift level under constant load weights (1 kg and 5 kg) using the Plantarray auto-calibration application.

The set-up was comprised of highly sensitive, temperature-compensated load cells, which were used as weighing lysimeters. Each controller was connected to its own control unit, which collected data and controlled irrigation. A 4-L pot containing a single plant in 20/30 sand (Negev Industrial Minerals Ltd., Israel) as growth medium was placed on each load cell. The numbers 20/30 refer to the upper and lower size of the mesh screen through which the sand was passed (20 = 20 squares across one linear inch of screen), resulting in a sand particle size of between 0.595- and 0.841-mm. Fertilizer (poly feed 17:10:27, Haifa Chemicals, Haifa, Israel) was supplied to the plants through the irrigation system (fertigation). The containers fit the pots tightly, to prevent evaporation, and had orifices at different heights on their side walls, to enable different water levels after drainage of excess water following irrigation. Evaporation from the pot surface was prevented by a cover with a circle cut out at its center through which the plant could grow. All pots were fertigated by four drippers, which were pushed into the upper part of the sand to ensure that the medium was wet evenly by each irrigation event. Fertigation was applied during the night in multi-pulses (i.e., the fertigation in the control treatment consisted of four irrigation pulses for 15 min, every 2 h to ensure proper leaching and the reaching of full pot water capacity).

Drought treatment

As each individual plant had a unique transpiration rate based on its size and location in the greenhouse, stopping the irrigation to all the plants at once would lead to a non-homogeneous drought treatment. To enable a standard drought treatment (i.e., similar drying rate for all pots), drought scenarios were automatically controlled via the system's feedback-irrigation controller. For the drought treatment, the system was set to irrigate each plant to 80% of its own previous day's transpiration, so that all plants would be subjected to the same gradual water stress [see Figure 3B in (Dalal et al., 2020)].

Measurement of quantitative physiological traits

The plant water-relations kinetics (recorded by the system every 3 min) and quantitative physiological traits of the plants were determined simultaneously for all plants (Figure 1), following (Halperin et al., 2017) with minor modifications. The examined traits were as follows: daily transpiration, transpiration rate (TR), whole-canopy stomatal conductance (Gsc) and biomass water-use efficiency (WUE_b). Cumulative transpiration (CT) was calculated as the sum of daily transpiration for all the days of the experiment for each plant.

Biomass water-use efficiency (WUE_b) was calculated by dividing the dry biomass weight of each plant by its CT at the end of the experiment, as defined in (Leakey et al., 2019). Daily weight gain was calculated by subtracting each day's pot weight from the pot weight measured on the previous day, both after reaching field capacity and full drainage at 04:00 [as described in detail in (Halperin et al., 2017)]. The plant's recovery from drought was described by the recovery of daily transpiration to its pre-drought level following the resumption of irrigation. The recovery rate was determined by comparing the amount of daily transpiration for 5 days after recovery.

Calculated volumetric water content (Cal. VWC) was derived from the mass balance difference of reserve water, soil wet weight, soil dry weight and soil volume (see Dalal et al., 2020).

Theta crit. (θ) is the point at which transpiration begins to be affected by limited soil water availability. It was determined by the piecewise linear fit of the transpiration rate and calculated VWC of the plants subjected to the drought treatment.

Stomatal density and aperture

A rapid imprinting method (Geisler and Sack, 2002) was used to determine stomatal apertures and density (Figures 8 and 9). Briefly, light-bodied vinyl polysiloxane dental resin (Heraeus-Kulzer; Hanau, Germany) was attached to the abaxial and adaxial sides of leaves and then removed after it had dried for 1 min. Mirror images of the resin imprints were made using nail polish. Once dried, the nail polish was removed from the resin epidermal imprints. The nail-polish imprints were mounted on microscope slides. A Leica DM500 microscope equipped with a 40x objective and a Leica ICC50W camera was used to observe and photograph the imprints at 20x and 60x magnification for stomatal density and apertures, respectively. The stomata in a field of view were counted at 20x magnification. Using the ImageJ software (http://rsb.info.nih.gov/ij/), stomatal images were analyzed to determine aperture size. A microscopic ruler (Olympus; Tokyo, Japan) was used for size calibration.

Statistical analysis

Continuous data were filtered and summarized using the SPAC analytic software embedded in the Plantarray system (PlantDitech, Yavne, Israel). All analyses were performed using the JMP® 15.0 Pro statistical package (SAS Institute, Cary, NC, USA)

unless otherwise specified. Box plots and continuous line graphs were generated using OriginPro, Version 2021 (OriginLab Corporation, Northampton, MA, USA).

Results

Field performance of the IL population

We started by analyzing two field experiments (from 2000, and 2004, see Table 1), which included 29 IL lines and M82. These plants were characterized for yield and biomass parameters, compared to the control M82 under optimal irrigation and water-limiting conditions (Figure 2). Under optimal irrigation, the lines were classified into high-yielder (HY), medium-yielder (MY) and low-yielder (LY) groups according to a comparison of their yields with that of M82: HY = >20% of M82 yield, MY = similar to M82 yield and LY = <20% of M82 yield. Based on the biomass of the different lines collected from the field at the end of the experiment relative to that of M82, the genotypes were also classified as having a high shoot biomass (HB, >20%), medium shoot biomass (MB, 20%) or low shoot biomass (LB, <20%; Table 1).

Based on the above classification and the terminology suggested by (Moshelion, 2020a), plant drought-response behavior was defined as follows: Plant resilience was measured as the plant's biomass relative to that of M82 under similar drought conditions and plant tolerance was measured as its TY under similar drought conditions. This means that, under similar drought stress, a line exhibiting higher biomass and higher yield would be classified as having a high-resilience (HR) and high-tolerance (HT) phenotype (HrHt). Conversely, a line with lower biomass and lower yield under drought conditions would be classified as have a low-resilience (LR) and low-tolerance (LT) phenotype (LrLt). If a line's biomass under stress was >20% of the control, but its yield

was lower than that of M82, it was defined as high-resilience–low-tolerance (HrLt; Table 1). This categorization resulted in 20 different groups ranging the spectrum from an ideotypic phenotype to a survival phenotype.

Six lines (marked with '*' in Table 1) and the M82 line were selected for further physiologic characterization using the functional telemetric platform. These seven genotypes were selected to represent a wide range of plant-response characteristics based on data from 4 to 5 years of well-irrigated field experiments and at least two years of data regarding performance under stress conditions. The selected lines were IL5-2, IL2-6, IL11-4, IL10-1, IL8-1 and IL8-1-3. IL5-2 performed better than M82 in terms of all parameters in both environments. It was an HY, HB, HT and HR (HyHbHtHr) line; it was ideotypic. IL2-6 was a high yielder under optimal irrigation, but a low-yielder under drought stress, while maintaining a high biomass under both conditions (HyHbLtHr). IL11-4 exhibited high yields under optimal irrigation, yet medium-level values for the rest of selection criteria (HyMbMtMr). IL10-1 showed good vegetative growth but had low yields under both wet and dry conditions. It was a low yielder with a high biomass, low tolerance and high resilience (LyHbLtHr). IL8-1 had low total yields and biomass under optimal irrigation and low yields under drought conditions, but medium biomass under drought stress (LySbLtMr). IL8-1-3 had low total yields and biomass under optimal irrigation and low yields under both optimal irrigation and drought conditions (LySbLtLr). We refer to its phenotype as a survival phenotype.

Physiological characterization of the selected genotypes

The midday A_N and g_s of 8-week-old plants of selected genotypes grown in sandy-loam soil in a semi-controlled greenhouse revealed no statistical differences between those genotypes (Supplemental Figure 1). There was a great deal of variability among the

results, which may have been caused by spatial and temporal differences in ambient conditions and the plant's physiological status between the measurements. Hence, we decided to measure all genotypes' water relations simultaneously and continuously.

All lines with four to eight biological replications revealed linear increases in transpiration over the period of optimal irrigation. On the first day of the experiment (4-week-old seedlings), no significant differences were observed between the lines (Figure 3 A, Day 1). However, differences between the lines soon developed. As the plants grew, some lines exhibited greater whole-plant transpiration (IL11-4 and IL5-2), while others exhibited medium to low levels of transpiration (IL8-1). After 18 days, all of the plants were subjected to controlled drought stress (a differential-feedback-irrigation drought treatment, see Materials and Methods), to expose them all to a similar drought-stress treatment in which soil volumetric water content (VWC) decreased at a similar rate (Figure 3 B), despite differences in their transpiration. Although all of the plants were exposed to a similar declining VWC, high-transpiring lines reached their VWC limitation point (θcrit.) more quickly and so reduced their transpiration earlier than the low-transpiring plants (Figure 4), revealing a transpiration-positional inversion (e.g., Figure 3 A, the transpiration flip-flop of IL11-4 and IL8-1).

Stress response and resilience evaluation

During the drought period, no differences in plant transpiration were observed between the lines (Figure 3 A), due to stomatal closure. It is very likely that other drought-defense mechanisms [e.g., reactive oxygen species (ROS) scavenging, embolism repair and prevention, etc.], were also activated, yet the estimation of these mechanisms' effectiveness across all of the plants and in real-time is very challenging in intact plants. Therefore, we tested the recovery rates of the different lines, assuming that the more effective these mechanisms, the faster the plants would recover. When the plants

reduced their transpiration to 10% of their maximum transpiration (Day 29), full irrigation was resumed and the plants' transpiration was monitored for 5 days. Over that period, IL5-2, IL11-4, IL10-1 and M82 showed rapid recovery (Figures 3A, 5A). The strong correlation between cumulative transpiration (CT) and the amount of dry biomass at the end of the experiment (which is an integral of the whole-plant transpiration kinetics over the entire 33-day period) revealed that the higher-biomass lines also transpired more than the smaller plants. We observed a linear relationship between cumulative transpiration and total biomass production (Figure 5 B). Moreover, the lines with the higher CT (IL5-2 and IL11-4) were also more efficient, in that they had higher water-loss to biomass-gain ratios (biomass water use efficiency, WUE_b) than the other lines (Figure 5 C) .

Daily whole-plant–environment kinetics

Despite the qualitative increases in daily transpiration, it was hard to discern a clear statistical difference between the lines based on their daily transpiration parameters. We assumed that differences in the momentary plasticity response to the ambient conditions (which were similar for all lines) over the course of the day might explain the differences in the performance of different lines. To understand the response of Gsc and the transpiration rate to ambient conditions, we monitored all of the lines simultaneously under optimal irrigation and drought conditions (50% of maximum midday transpiration, after θcrit., Day 23 of the experiment, Figures 6 and 7). Under well-irrigated conditions (Day 16 of the experiment), the whole-canopy Gsc and TR revealed a similar response pattern to light and VPD across the different lines. All lines opened their stomata in accordance with PAR and VPD, increasing their Gsc and TR from 06:00 to 10:00 (Figure 6). Daily maximum Gsc and RT were relatively stable at midday (10:00 to 14:00) and until the late afternoon, as were the PAR and VPD. In the

late afternoon, there were sharp declines in Gsc according to PAR, while TR increased following the VPD pattern. With the drop in VPD, transpiration also decreased (Figure 6C). This shows that during the afternoon and evening hours, the WUE of the plants was at its lowest level. The transpiration rate had a pattern similar to that of the daily transpiration shown in Figure 3 A, but canopy conductance had a different pattern, as it was normalized to plant weight. Unlike the situation under optimal-irrigation conditions, the Gsc and TR kinetics of the plants exposed to soil water-limiting conditions differed between the different lines and in response to PAR and VPD (which were very similar to the pre-stress conditions, see Supplemental Figure 2). All lines experienced reductions in Gsc and TR from late morning-noon, regardless of the ambient PAR and VPD conditions. However, the high-performing lines (i.e., IL5-2 and IL11-4) presented a different response pattern, with relatively high Gsc (Figure 7 A and B) in the morning (6:00 to 10:00) and a relatively low transpiration rate (Figures 7 a and b) at the same time, followed by an immediate and linear reduction in those parameters during the middle of the day and the afternoon (10:00 to the evening hours), suggesting a possibly higher WUE for this period, as compared to other lines. On the other hand, low-performing lines (i.e., IL10-1, IL8-1 and IL8-1-3) presented lower Gsc during the early hours (when VPD is low) and reached their Gsc peaks later in the day (Figure 7 E, F and G, respectively) and those peaks persisted for longer periods, causing those plants to lose more water to transpiration (Figure 7 e, f and g respectively). In these high-resolution measurements of Gsc and Tr patterns, we detected differences between lines that were not evident in the low-resolution measurements of daily transpiration (i.e., no differences between lines were detected in the daily-transpiration stress response unlike the pre-stress period; Figure 3 A). To better understand the

different Gsc response patterns of the high-yielding lines, we examined their stomatal densities and apertures.

Variation in stomatal morphology among the lines

Measurements of stomatal density and apertures revealed that lines IL5-2, IL11-4, IL8-1-3 and IL10-1 had higher abaxial stomatal densities than adaxial stomatal densities. In contrast, the other lines had similar stomatal densities on the two sides of their leaves. No differences were observed in the maximal stomatal aperture size between the abaxial and adaxial leaf sides for each line, apart from M82 and IL8-1-3, which had larger stomatal apertures on the abaxial and adaxial sides of their leaves, respectively (Figure 8 B). Nevertheless, each line had its own maximum aperture for both abaxial and adaxial sides of its leaves at different times of day (Figure 9). Specifically, IL5-2 reached its maximal abaxial peak aperture around 07:00 and its maximal adaxial peak aperture around 10:00 (Figure 9 A, a). M82 reached both its maximal abaxial and adaxial apertures around 10:00. Lines IL8-1, IL11-4 and IL10-1 revealed maximum aperture on both their adaxial and abaxial sides around 13:00. However, while the stomatal apertures of IL10-1 and IL11-4 became smaller after they peaked, IL8-1 maintained its large apertures until 17:00. Line 8-1-3 maintained consistently small apertures throughout the day, with slightly larger apertures in the afternoon on the adaxial side of its leaves (Figure 9 G and g).

Abaxial, but not adaxial stomatal density is correlated with the transcription of stomatal development candidate genes

We examined the relationship between transcriptome data generated by (Chitwood et al., 2013) and the abaxial and adaxial stomatal densities that we measured. We found

that the expression levels of the genes SPEECHLESS (*SPCH*) was strongly and positively correlated with abaxial stomata density (Figure 10 B and C). Zeaxanthin epoxidase gene **(***ZEP*) was strongly negatively correlated with abaxial stomatal density (Figure 10 E and F).

Discussion

Yield and biomass data are single, endpoint traits usually used to distinguish between different genotypes grown in the field. These data are the cumulative result of multiple G×E interactions over the course of the growing season and, therefore, may vary between different locations and years (van Eeuwijk et al., 2019). This complexity poses a major challenge for crop-phenotype studies (Momen et al., 2019). To overcome some of these challenges, we chose seven different genotypes and examined at least four years of field data. The lines could be categorized as high-yielders (IL5-2, IL11-4 and Il2-6), a medium-yielder (similar to M82) or low-yielders (IL8-1, IL10-1 and 8-1-3) and were continuously and simultaneous compared with one another and with a control (i.e., M82) under identical atmospheric conditions in optimal-irrigation, drought-stress and recovery scenarios. To the best of our knowledge, this is the first physiological phenotyping study to incorporate multiple years of field performance of many genotypes.

Since leaf photosynthesis has been reported to be the most important trait for yield improvement (Du et al., 2020; Tatsumi et al., 2020), we first used a manual gas-exchange apparatus to measure the AN and g_s of the selected lines (Supplemental Figure 1). Although we saw some trends, we did not see any significant differences that could explain the differences in yield performance among these lines. This could be related to the relatively low sample size we could measure within the 2-h period between

10:00–12:00, namely, only three biological replications of each for the seven genotypes with a time gap of ~40 min between the three replications due to the nature of the measurement. Yet even within this short time, environmental conditions such as levels of sunlight, temperature and VPD did not remain constant. Therefore, it is likely that low frequency, manual measurements — even of a critical trait such as A_N — are less likely to yield data that can be used to answer good selection criteria as the measured values differ under natural, constantly fluctuating environment conditions (Sakoda et al., 2020).

The primary challenge of G×E phenotyping is detecting the small behavioral differences between different lines under similar environmental conditions, which, over time, have a cumulative effect on crop yield (Moshelion, 2020; Gosa et al., 2022). The sampling of longitudinal (or continuous) traits [i.e., traits that are measured repeatedly over time (Yang et al., 2006)] is necessary to determine the mechanisms by which the environment influences the plant's performance. As reviewed in (Moreira et al., 2020), the ability to measure a crop's longitudinal traits holds promise for better describing its dynamic nature. In agreement with this approach, performing continuous measurements instead of traditional single-point measurements was shown to improve the accuracy of the longitudinal trait prediction model for plant shoot growth and to aid the discovery of loci associated with shoot growth trajectories. (Campbell et al., 2019). To understand the dynamic trajectory responses of the different lines, continuous measurement of the soil-plant-atmosphere continuum (SPAC) conditions may be more informative than single time-point measurements. Here, we monitored the longitudinal traits of daily transpiration and Gsc at a minute resolution, along with SPAC, throughout the growth period. We noticed that even under optimal irrigation, single-point measurements of daily transpiration could be misleading as differences started to emerge over the course

of the growth period, suggesting that a single-point measurement during the early growth phases might not provide very much useful information and underscoring the importance of identifying the appropriate time axis for the evaluation of any measurement data.

One additional challenge with the dynamic trajectory response is the need to compare different lines at similar levels of drought stress, as different plants exhibit different water-consumption behavior. The pursuit of a better understanding of trait dynamics under water-deficit conditions is among the biggest challenges in breeding for higher yields under drought conditions (Sinclair, 2011; Snowdon et al., 2020). Designing a standard, repeatable and reliable drought experiment and screen is among the most challenging tasks (Moshelion, 2020). In this study, we actively maintained similar drought treatments for all lines simultaneously (Figure 3B) by defining the initial drought-stress point in terms of each plant's θcrit., as a standard drought evaluation point (Figure 4). Unlike the high-transpiring plants (e.g., see, IL5-2, IL11-4; Figure 3A), the smaller, low-transpiring plants (e.g., IL8-1; Figure 3A) exhibited smaller reductions in their daily transpiration in response to the same drought treatment. Therefore, during the drought treatment, even though similar water content was automatically maintained for all lines (Figure 3 B), we observed a transpiration-positional inversion between the low- and high-transpiring plants (Figure 3 A, "transpiration flip-flop").

This result illustrates the true challenges of the commonly used method of closing irrigation taps for a few days to study drought stress, especially when plants of different sizes and sensitivities to environmental conditions are involved. This result clearly shows the importance of taking caution when using the commonly used method developed by (Michael D. Snow and David T. Tingey, 1985) to study water stress,

particularly when the experiment involves a variety of plant behaviors. The use of θcrit. as a standard drought evaluation point (see Figure 4) could help to overcome this challenge. θcrit. is also important for showing the dynamics and sensitivity of a plant to stress, by showing how quickly the high-transpiring plants can reduce their transpiration, which could affect their stress tolerance. For example, as shown in Figure 4, IL5-2 and IL11-4 reached the θcrit. point more quickly than the other lines. This indicates that those lines are opportunistic as they transpire and produce more at optimum levels under full irrigation and close their stomata as soon as they sense a water deficit.

Under stress, plants generally switch from a productive mode to a survival mode. That switch includes longitudinal physiological, anatomical and biochemical adaptations (Kerchev and van Breusegem, 2021). Recovery from drought stress is the ability to return to initial pre-stress levels of growth and physiological functioning once soil water content has been restored. Although resilience is just as important as stress response, it has received less attention (Guo et al., 2020), possibly due to the difficulty of characterizing it.

As shown in Figure 5 A, the examined lines exhibited differences in their ability to return to their pre-stress levels of daily transpiration, as compared to their daily transpiration over the first 5 days after irrigation was resumed. The lines with the highest levels of transpiration before the stress treatment (IL5-2, IL11-4) recovered rapidly after the drought. This was contrary to our hypothesis that higher-transpiring plants would be more susceptible to drought and recover relatively slowly. Similarly, these lines were classified as highly resilient and medium resilient in the field (Table 1) and showed faster stomatal closure, higher $\theta_{crit.}$ (Figure 4), higher WUE_b (Figure 5c)

and relatively high Gsc to TR under drought conditions (Figure 7 A, a and B, b, respectively), indicating the importance of a quick and dynamic response to water stress.

Based on these results, we conclude that stress-adaptation mechanisms that are challenging to detect during the stress period may contribute to plant resilience. This finding is consistent with a previous report concerning maize (Chen et al., 2016), which showed that drought recovery is an important part of whole plant growth under water-stress conditions. Using a method for detecting drought-stress resilience at an early growth stage in conjunction with a field trial may allow the prediction of resilience at earlier growth stages. This approach could also be a way to detect genetic variability in novel mechanisms of tolerance. If combined with field testing (Chapuis et al., 2012), data should be collected during both the vegetative and the reproductive phase of the plants' growth, since plants tend to respond differently to stress during those different growth phases (Gosa et al., 2022) (Chen et al., 2016).

Dynamic water-use efficiency: The morning stomatal peak under water-deficit conditions

Plants exhibit dynamic water-use regulation throughout the growing season in response to VPD changes. The temporal dynamics of water-use traits substantially increases productivity (Sinclair, 2018)**.** Similar to seasonal variation, diurnal VPD is also dynamic, which affects plant responses momentarily (Figure 6). Yet, in the absence of SWC limitations, all lines demonstrated similar response patterns, differing only in their absolute values. Under limiting SWC, different lines exhibited different responses to VPD and PAR (Figure 7 and Supplemental Figure 2), suggesting that some dynamic responses could be more beneficial than others in certain environments. An example of

such beneficial dynamic responses can be seen in the early morning stomatal conductance peaks of the high-yielding lines. Under drought conditions, IL5-2 and IL11-4 (Figure 7 A and B) maintained relatively high stomatal conductance when PAR was relatively high, but VPD was still low, which resulted in a relatively low rate of water loss to transpiration (Figure 7 a and b). This kind of opportunistic stomatal behavior has been reported in the most water stress-tolerant forest plants such as *Acacia* and hemiparasitic mistletoes (Loranthus europaeus (LE)) (Ullmann et al., 1985; Resco de Dios et al., 2016), a high-yielding wheat (Triticum durum cv) introgression line (Bacher et al., 2021), soybean (*Glycine max*) (TEARE and KANEMASU, 1972) and *Arabidopsis thaliana* (Hassidim et al., 2017). Although all of these studies documented the existence of this stomatal morning-rise phenotype, it was an anticipative hypothesis that the phenotype would increase productivity and fitness under drought using the photosynthetically active radiation (PAR), which could lead to increased CO_2 assimilation (Schoppach et al., 2020). In a recent study, we showed that this kind of early morning Gsc peak, described as the "golden hour" (Gosa et al., 2019), is strongly correlated with tomato yield in the field (Gosa et al., 2022).

Our current findings confirm the importance of this early morning stomatal peak and also point to genetic variability leading to this important trait. Specifically, the two high-yielding lines were IL5-2 and IL11-4, which are otherwise very different from one another. Moreover, these lines also exhibited high WUE_b, high shoot dry weights (Figure 4) and medium to high drought tolerance in the field (Table 1). In contrast, another high-yielding line, IL2-6, presented very different daily Gsc–Tr kinetics, which were similar to those of the low-yielding Il8-1 (Figure 7). IL2-6 also had low WUE_b and low shoot dry weights (Figure 4), as well as low drought tolerance in the field

(Table 1). That is, this different combination of various traits resulted in a similar outcome.

In recent years, several studies have suggested stomatal functional anatomy mechanisms as a promising target for improving productivity and resilience (Sakoda et al., 2020b; Sultana et al., 2021). For instance, high stomatal density has been suggested as a safety efficiency trade-off; as it shows greater sensitivity to closure during leaf dehydration (Henry et al., 2019). An addition mechanism reported as a good proxy for productivity and WUE is the ratio between the stomatal densities on the abaxial and adaxial sides of a plant's leaves (Muir et al., 2014).

In fact, our results revealed different combinations of both in the different IL lines. All of the IL lines that we tested had similar total stomatal densities. However, higher stomatal densities on the abaxial side were observed among both high-yielding lines (L5-2 and IL11-4) and low-yielding lines (IL10-1 and IL 8-1-3; Figure 8 A). In addition, other high-yielding lines, M82 and IL2-6 had stomatal densities and stomatal ratios that were similar to those of the low-yielding IL8-1 (Figure 8 A).

These findings raise more questions about the roles of stomatal ratio and stomatal density in Gsc regulation. Although, the abaxial stomata seem to play important roles in light sensitivity, photosynthesis, and WUE (TURNER, 1970; Driscoll et al., 2006; Wang et al., 2008; Lei et al., 2018), the actual relative contribution of the abaxial and adaxial leaf sides to crop productivity remains unclear as it depends on several factors such as the position of light illumination in the greenhouse, wind movement in the field and crop type (Zhang et al., 2016; Paradiso et al., 2020). We suggest that, in tomato, the combination of stomatal ratio, stomatal density and the sensitivity of the conductance of the stomata on each side of the leaves to the ambient conditions is the key to understanding a genotype's adaptation to a particular environment (G×E

optimization), its resilience and its WUE. For example, both IL8-1 and IL8-1-3 were very low in all productive and resilient field-based parameters (Table 1). Indeed, their daily transpiration levels were low and despite their shorter exposure to stress, they were the last to recover (Figure 3). Both lines exhibited similar low shoot dry biomass and low WUE_b (Figure 5). Moreover, under stress, both exhibited similar patterns of daily Gsc (Figure 7 E and G) and Tr rates (Figure 7 e and g). However, these similar response patterns result from different stomatal ratios and stomatal densities (Figure 8 A) and maximal stomatal apertures at different times of the day (Figures 8 B and 9 D, G, d and g). Specifically, IL8-1 had a lower stomatal density, yet larger stomatal apertures on the adaxial sides of its leaves, which have more exposure to the atmosphere during the highest VPD hours. It maintained those large apertures for a longer time (Figure 9 d), resulting in a transpiration rate that was similar to that of IL8-1-3 (Figure 7 e and g), which had a higher stomatal density and stomatal ratio (Figure 8), yet lower daily aperture kinetics on both the abaxial and adaxial sides of its leaves (Figure 9 G and g).

On the other hand, IL5-2, which we categorized as the idiotype (high levels of all productivity and resilience parameters; Table 1), exhibited high levels of daily transpiration, despite the fact that it was exposed to the drought stress for a longer period of time (earlier θcrit.; Figure 4). Plants of this line also recovered the most quickly (Figure 3 A) and had high levels of dry biomass and WUE_b (Figure 5 C). Accordingly, under stress, this line exhibited a high Gsc, but low Tr rates (Figure 7 A and a) due to an earlier aperture peak (Figure 9 A). Line IL11-4 was almost identical to IL5-2 in all parameters, including a similar stomatal ratio and stomatal density (Figure 8 A), yet it had a later aperture peak (Figure 9 B and b) at a higher VPD. This “risk-taking” may reflect its medium shoot weight, tolerance and resistance in the field.

The other lines (i.e., M82 and IL2-6) were similar in their daily transpiration, dry biomass, WUE_b, θcrit., daily Gsc and TR patterns and stomatal ratios (Figures 3, 4, 5, 7 and 8, respectively). However, IL2-6 had a lower stomatal density (Figure 8) and larger adaxial stomatal apertures late in the afternoon, which could explain why it was slower to recover (Figure 3 A) and could be related to its medium level of tolerance under field conditions. IL10-1 was also similar to M82 in its daily transpiration, dry biomass, WUE_b, θcrit., stomatal density and adaxial–abaxial stomatal aperture ratio (Figures 3, 4, 5, 8 and 9, respectively), yet IL10-1 had a higher stomatal ratio (Figures 8) and much higher daily Gsc and TR under drought conditions (Figure 7 F and f). These patterns could be related to its low tolerance in the field (Table 1). IL8-1-3 had a stomatal density and stomatal ratio that were similar to those of the high-yielding IL5-2 (Figure 8 A), but it exhibited low transpiration (Figure 3 A) and low yield in the field (Table 1). This could be explained by the fact that this line had relatively small stomatal apertures on both sides of its leaves (Figures 8 B and 9 G and g). Together, these findings indicate that the combination of stomatal density, stomatal ratio, daily stomatal-aperture profile and maximal stomatal apertures is crucial for plant adaptation and productivity under water-stress conditions.

To shade some light on the possible genetic basis of this stomatal trait variation as a potential target for future study, we used transcriptome data for these tomato lines generated by (Chitwood et al., 2013) and observed a correlation between two of the stomatal development related genes and abaxial and adaxial stomatal density. These genes are SPEECHLESS (*SPCH* Solyc03g007410.2.1) and a gene that encodes zeaxanthin epoxidase (*ZEP*, Solyc02g090890.2.1).

SPCH is a signal integrator, which combines intralineage signals and accepts hormones and effects of the environment during development to regulate stomatal density and

patterning (Chen et al., 2020). Zeaxanthin epoxidase (*ZEP*) is involved in the biosynthesis of abscisic acid and the xanthophyll cycle and plays an important role in regulating plant responses to various environmental stresses (Lou et al., 2017). Interestingly, we could see a strong positive relationship between abaxial stomatal density and the expression of the stomatal developmental gene, *SPCH*, whereas the correlation between adaxial stomatal density and *SPCH* expression was less pronounced (Figure 10 C and D). On the other hand, we also observed a strongly negative correlation between abaxial stomatal density and *ZEP* expression. *ZEP* was expressed at a very low level in IL5-2, the most plastic line in this study (Figure 10 D–F). Although our current work did not involve the elucidation of genetic mechanisms, we believe that these observed correlations will stimulate future study and help to spur researchers to delve into this subject, to learn how stomatal ratios can be used to improve crop plasticity in a constantly changing environment.

In conclusion, plants with high levels of transpiration can be more productive in the absence of water limitations. However, the key to maximizing productivity under SWC constraints is to maximize stomatal aperture when VPD is low, quickly close stomata when VPD increases and/or SWC decreases and then rapidly open stomata when SWC increases. Still, continuous measurement of stomatal apertures is not feasible as part of a phenotypic scan. Similarly, it is also not feasible to measure stomatal conductance with a manual, steady state, gas-exchange apparatus due to the limited areas these machines measure (usually a leaf), which does not reflect the functional anatomy of the whole plant (including the abaxial-adaxial stomatal density ratio, leaf structure and canopy phyllotaxis, as well as other factors). On the other hand, whole-plant measurement by the gravimetric method provides an absolute measurement of the response of the whole plant to environmental changes, which can be useful in a high-

625 throughput screening for either forward or reverse G×E phenotyping. This could
626 contribute immensely to breeding programs focused on improving crop performance in
627 different climates.

628

629 **Acknowledgements**

630 This research was supported by the ISF-NSFC joint research program (grant no.
631 2436/18), as well as the Israel Science Foundation (grant no. 1043/20) and the Israel
632 Ministry of Agriculture and Rural Development (Eugene Kandel Knowledge Centers)
633 as part of the Root of the Matter: The Root Zone Knowledge Center for Leveraging
634 Modern Agriculture. We thank Prof. Dani Zamir at our institute for providing us with
635 the IL seeds and multiple years of field-based yield data for the lines used in this study.

636

637 **Author Contributions**

638 Sanbon Chaka Gosa planned, conducted, and analyzed all the experiments, wrote this
639 thesis except the following:
640 Bogale Abebe and Ravitesjes Patil took part conducting the lysimeter experiments
641 Ramon Manica took part in stomatal imprint and leaf gas exchange experiments
642 Moshelion M: corresponding author, supervised, planned wrote the MS together with
643 Sanbon Gosa in all the results in this work.

644

645

646

647 **Legends**

648 **Table 1.** Reverse phenotypic classification of tomato introgression lines based on total
649 yield and plant weight under well-irrigated and dry field conditions (as presented in Fig.

2). Relative to M82, lines were classified into three groups based on their fruit weights: high-yielders (HY, >20%), low-yielders (LY, 20%) and medium-yielders (MY, similar). Similarly, lines were classified as high biomass (HB), medium biomass (MB) and small biomass (SB), relative to M82. Lines with all "highs" were considered ideotypic. The drought stress-response phenotype was classified based on terminology suggested by Moshelion (2020). Specifically, under drought conditions a line with a fruit weight that was 20% higher fruit than that of M82 was classified as having a high tolerance (HT), a line with a fruit weight that was 20% lower than that of M82 was classified as having a low tolerance and lines with fruit weights similar to that of M82 were classified as having moderate tolerance (MT). Plants that maintained or increased their biomass under stress were categorized as having a high resilience (HR). Plants that maintained or reached medium levels of shoot biomass were classified as medium resilience (MR). Small plants that maintained their size or larger plants that lost biomass under stress were classified as having low resilience (LR); the former phenotype was also referred to as a survival phenotype. We identified 20 classification groups; seven of which (marked with *) were selected for further physiologic characterization using the functional telemetric platform. All of these lines exhibited consistent behavior across the years of study data.

Figure 1. Overview of the telemetric, gravimetric phenotyping platform and analysis scheme. A, A partial view of multiple tomato introgression lines positioned on the Plantarray screening platform [located at the Israeli Center of Research Excellence (ICORE) for Plant Adaptation to the Changing Environment, at The Hebrew University of Jerusalem]. B, Randomized experimental setup of all plants simultaneously measured. Different colors represent different lines and treatments. C, An illustration of the direct soil-plant-atmosphere measurements taken for a single plant. The

675 continuous data from the Plantarray system is uploaded to the internet server in real
676 time. D, Graphic presentation of the absolute values of the continuous atmospheric data
677 of vapor pressure deficit (VPD, red line) and photosynthetically active radiation (PAR,
678 blue line) over time. E, Whole-plant daily transpiration kinetics. F, Plant weight gain
679 over time G, soil moisture content over time. Each line represents the continuous
680 measurement of individual plants throughout the experiment period.

681 **Figure 2.** Field performance of 29 tomato introgression lines (gray) and the M82
682 control (black). A, Two years of mean fruit weights (ranked from low to high) under
683 well-irrigated conditions. B, Two years of mean fruit weights (ranked from low to high)
684 under drought conditions. C, Two years of mean shoot weights at harvest (ranked from
685 low to high) under well-irrigated conditions. D, Two years of mean shoot weights at
686 harvest (ranked from low to high) under drought conditions. The square (□) in the box
687 plot represents the mean value. The box-splitting horizontal bands indicates the sample
688 median and bars show the interquartile range (25th to 75th percentile). Points below or
689 above the interquartile ranges are outliers respectively.

690 **Figure 3.** A, Daily transpiration of tomato seedlings over the entire experimental
691 period. Data points are means ± SE of continuous daily whole-plant transpiration over
692 the entire experimental period (32 days). B, Mean ± SE volumetric water content
693 (VWC) measured by a soil probe over the course of the experiment. The drought
694 treatment was followed by a recovery period followed during which the resumed
695 irrigation brought the pot back to full capacity. Groups were compared using Tukey's
696 Honest Significance test; different letters above points represent significant differences
697 between lines; $p < 0.05$. $n = 5–8$ plants per group.

Figure 4. The physiological drought point (θcrit.) was determined as the point at which soil water is restricted from supplying mid-day transpiration needs, for all of the plants presented in Fig. 3. This point was identified using piecewise correlations based on the relationships between two segmented lines that intersected (following Halperin et al., 2016). The yellow box in the middle represents the standard drought-evaluation zone, in which the performance of all lines was evaluated under drought stress.

Figure 5. A, Transpiration recovery rate for five days after the resumption of irrigation in seven different tomato lines. B, Correlation between shoot dry weight and cumulative daily transpiration for 33 days during the screening period. Data points are the means ± SE (n = 5–8). C, Means ± SE of biomass WUE of the different lines (calculated by dividing the dry biomass weight by the cumulative transpiration of each plant).

Figure 6. Daily patterns of A, PAR (black line) and VPD (red line), B, whole-canopy conductance and C, whole-canopy transpiration rate, as continuously measured under well-irrigated conditions. Data are means ± SE; n = 5–8.

Figure 7. Daily variation in canopy conductance and transpiration rate under drought-stress conditions. Whole-canopy conductance (A–G) and transpiration rate (a–g) measured continuously. Representative days were shown for the stress after the θcrit. point (yellow block in Fig. 4). Data are shown as means ± SE (n = 3–8).

Figure 8. Leaf stomatal traits of the different tomato lines. A, Total (gray), abaxial (lower leaf side, light green) and adaxial (upper leaf side, dark green) stomatal densities of six introgression lines of tomato and M82. Data are derived from three technical and three biological replications imaged at their central lamina. The box-splitting horizontal bands indicate sample medians, the square box in the middle indicates the mean, and bars show the interquartile range (25th to 75th percentile), points below or above the

722 interquartile ranges are outliers. B, Total stomatal apertures of the same lines (pore
723 width, μm). * Indicates a significant difference between the abaxial and adaxial sides
724 of an individual line, according to Student's *t*-test. Different letters indicate
725 significantly different means (capital letters for total stomatal density, and light green
726 lower-case letters for the abaxial side of the leaves and dark green lower-case letters for
727 the adaxial side), according to Tukey's Honest Significance test ($p < 0.05$).

728 **Figure 9.** Daily variation in, A–G, abaxial stomatal apertures and, a–g, adaxial stomatal
729 apertures. The broken lines indicate the maximum aperture during the daytime. The
730 square (□) in the box plot represents the mean value. The box-splitting horizontal bands
731 indicate sample medians and bars show the interquartile range (25th to 75th percentile).
732 Points below or above the interquartile ranges are outliers. The dashed lines in each
733 figure indicate the point in the day at which the apertures were largest.

734 **Figure 10.** Expression of genes related to stomatal development correlated to abaxial
735 and adaxial stomatal distribution. A, *SPCH* expression in the different lines. B,
736 Relationship between *SPCH* expression and abaxial stomata density. C, Relationship
737 between *SPCH* expression and adaxial stomatal density. D, *ZEP* expression in the
738 different lines. E, Relationship between *ZEP* expression and abaxial stomatal density.
739 F, Relationship between *ZEP* expression and adaxial stomatal density. The gene-
740 expression data are from Chitwood et al. (2013).

741 **Supplementary Figure 1.** Leaf gas exchange of different tomato introgression lines
742 under well-irrigated greenhouse conditions. A, Rate of carbon assimilation in young
743 leaves before flowering. B, Stomatal conductance of young leaves before flowering.
744 The square (□) in the box plot represents the mean value. The box-splitting horizontal
745 bands indicate sample medians and bars show the interquartile range (25th to 75th

746 percentile), points below or above the interquartile ranges are outliers. **Supplementary**
747 **Figure 2.** Daily patterns PAR (black line) and VPD (red line) during the period of
748 water-deficit conditions.

749

750 **References**

751 **Bacher H, Sharaby Y, Walia H, Peleg Z** (2021) Modify Root/Shoot ratio Alleviate Root
752 Water Influxes in Wheat under Drought Stress. Journal of experimental botany .
753 doi: 10.1093/jxb/erab500/6429243

754 **Campbell M, Momen M, Walia H, Morota G** (2019) Leveraging Breeding Values
755 Obtained from Random Regression Models for Genetic Inference of Longitudinal
756 Traits. The Plant Genome. doi: 10.3835/plantgenome2018.10.0075

757 **Chapuis R, Delluc C, Debeuf R, Tardieu F, Welcker C** (2012) Resiliences to water
758 deficit in a phenotyping platform and in the field: How related are they in
759 maize? European Journal of Agronomy **42**: 59–67

760 **Chazdon RL, Pearcy RW** (1986) Photosynthetic responses to light variation in
761 rainforest species - II. Carbon gain and photosynthetic efficiency during
762 lightflecks. Oecologia. doi: 10.1007/BF00410358

763 **Chen D, Wang S, Cao B, Cao D, Leng G, Li H, Yin L, Shan L, Deng X** (2016) Genotypic
764 variation in growth and physiological response to drought stress and re-
765 watering reveals the critical role of recovery in drought adaptation in maize
766 seedlings. Frontiers in Plant Science. doi: 10.3389/fpls.2015.01241

Chen L, Wu Z, Hou S (2020) SPEECHLESS speaks loudly in stomatal development. Frontiers in plant science **11**: 114

Chitwood DH, Kumar R, Headland LR, Ranjan A, Covington MF, Ichihashi Y, Fulop D, Jiménez-Gómez JM, Peng J, Maloof JN, et al (2013) A quantitative genetic basis for leaf morphology in a set of precisely defined tomato introgression lines. Plant Cell. doi: 10.1105/tpc.113.112391

Claeys H, Inzé D (2013) The agony of choice: How plants balance growth and survival under water-limiting conditions. Plant Physiology **162**: 1768–1779

Dalal A, Shenhar I, Bourstein R, Mayo A, Grunwald Y, Averbuch N, Attia Z, Wallach R, Moshelion M (2020) A telemetric, gravimetric platform for real-time physiological phenotyping of plant–environment interactions. Journal of Visualized Experiments. doi: 10.3791/61280

Driscoll SP, Prins A, Olmos E, Kunert KJ, Foyer CH (2006) Specification of adaxial and abaxial stomata, epidermal structure and photosynthesis to CO2 enrichment in maize leaves. Journal of Experimental Botany. doi: 10.1093/jxb/erj030

Du T, Meng P, Huang J, Peng S, Xiong D (2020) Fast photosynthesis measurements for phenotyping photosynthetic capacity of rice. Plant Methods. doi: 10.1186/s13007-020-0553-2

Durand M, Brendel O, Buré C, le Thiec D (2019) Altered stomatal dynamics induced by changes in irradiance and vapour-pressure deficit under drought: impacts on the whole-plant transpiration efficiency of poplar genotypes. New Phytologist. doi: 10.1111/nph.15710

Duursma RA, Blackman CJ, Lopéz R, Martin-StPaul NK, Cochard H, Medlyn BE (2019) On the minimum leaf conductance: its role in models of plant water use, and ecological and environmental controls. New Phytologist. doi: 10.1111/nph.15395

van Eeuwijk FA, Bustos-Korts D, Millet EJ, Boer MP, Kruijer W, Thompson A, Malosetti M, Iwata H, Quiroz R, Kuppe C, et al (2019) Modelling strategies for assessing and increasing the effectiveness of new phenotyping techniques in plant breeding. Plant Science. doi: 10.1016/j.plantsci.2018.06.018

Eshed Y, Zamir D (1995) An introgression line population of Lycopersicon pennellii in the cultivated tomato enables the identification and fine mapping of yield-associated QTL. Genetics

FAO (2017) The Future of Food and Agriculture. Fao

Fridman E, Pleban T, Zamir D (2000) A recombination hotspot delimits a wild-species quantitative trait locus for tomato sugar content to 484 bp within an invertase gene. Proceedings of the National Academy of Sciences of the United States of America. doi: 10.1073/pnas.97.9.4718

Furbank RT, Tester M (2011) Phenomics - technologies to relieve the phenotyping bottleneck. Trends in Plant Science **16**: 635–644

Gao C (2021) Genome engineering for crop improvement and future agriculture. Cell. doi: 10.1016/j.cell.2021.01.005

Geisler MJ, Sack FD (2002) Variable timing of developmental progression in the stomatal pathway in Arabidopsis cotyledons. New Phytologist. doi: 10.1046/j.0028-646X.2001.00332.x

Ghanem ME, Marrou H, Sinclair TR (2015) Physiological phenotyping of plants for crop improvement. Trends in Plant Science **20**: 139–144

Gosa SC, Koch A, Shenhar I, Hirschberg J, Zamir D, Moshelion M (2022) The potential of dynamic physiological traits in young tomato plants to predict field-yield performance. Plant Science. doi: 10.1016/j.plantsci.2021.111122

Gosa SC, Lupo Y, Moshelion M (2019) Quantitative and comparative analysis of whole-plant performance for functional physiological traits phenotyping: New tools to support pre-breeding and plant stress physiology studies. Plant Science. doi: 10.1016/j.plantsci.2018.05.008

Guo T, Tian C, Chen C, Duan Z, Zhu Q, Sun LZ (2020) Growth and carbohydrate dynamic of perennial ryegrass seedlings during PEG-simulated drought and subsequent recovery. Plant Physiology and Biochemistry **154**: 85–93

Gur A, Zamir D (2004) Unused natural variation can lift yield barriers in plant breeding. PLoS Biology. doi: 10.1371/journal.pbio.0020245

Halperin O, Gebremedhin A, Wallach R, Moshelion M (2017) High-throughput physiological phenotyping and screening system for the characterization of plant???environment interactions. Plant Journal **89**: 839–850

Hassidim M, Dakhiya Y, Turjeman A, Hussien D, Shor E, Anidjar A, Goldberg K, Green RM (2017) CIRCADIAN CLOCK ASSOCIATED1 (CCA1) and the circadian control of stomatal aperture. Plant Physiology. doi: 10.1104/pp.17.01214

Henry C, John GP, Pan R, Bartlett MK, Fletcher LR, Scoffoni C, Sack L (2019) A stomatal safety-efficiency trade-off constrains responses to leaf dehydration. Nature Communications. doi: 10.1038/s41467-019-11006-1

Hetherington AM, Woodward FI (2003) The role of stomata in sensing and driving environmental change. Nature. doi: 10.1038/nature01843

Kerchev PI, van Breusegem F (2021) Improving oxidative stress resilience in plants. Plant Journal. doi: 10.1111/tpj.15493

Leakey ADB, Ferguson JN, Pignon CP, Wu A, Jin Z, Hammer GL, Lobell DB (2019) Annual Review of Plant Biology Water Use Efficiency as a Constraint and Target for Improving the Resilience and Productivity of C 3 and C 4 Crops. Annu Rev Plant Biol **70**: 781–808

Lei ZY, Han JM, Yi XP, Zhang WF, Zhang YL (2018) Coordinated variation between veins and stomata in cotton and its relationship with water-use efficiency under drought stress. Photosynthetica. doi: 10.1007/s11099-018-0847-z

Lou Y, Sun H, Li L, Zhao H, Gao Z (2017) Characterization and Primary Functional Analysis of a Bamboo ZEP Gene from Phyllostachys edulis. DNA and Cell Biology. doi: 10.1089/dna.2017.3705

Massonnet C, Vile D, Fabre J, Hannah MA, Caldana C, Lisec J, Beemster GTS, Meyer RC, Messerli G, Gronlund JT, et al (2010) Probing the reproducibility of leaf

growth and molecular phenotypes: A comparison of three Arabidopsis accessions cultivated in ten laboratories. Plant Physiology. doi: 10.1104/pp.109.148338

Matthews JSA, Vialet-Chabrand SRM, Lawson T (2017) Diurnal variation in gas exchange: The balance between carbon fixation and water loss. Plant Physiology. doi: 10.1104/pp.17.00152

Michael D. Snow and David T. Tingey (1985) Evaluation of a System for the Imposition of Plant Water Stress. Plant Physiol **Mar; 77**: 602–607

Mir RR, Reynolds M, Pinto F, Khan MA, Bhat MA (2019) High-throughput phenotyping for crop improvement in the genomics era. Plant Science. doi: 10.1016/j.plantsci.2019.01.007

Momen M, Campbell MT, Walia H, Morota G (2019) Predicting longitudinal traits derived from high-throughput phenomics in contrasting environments using genomic Legendre polynomials and B-splines. G3: Genes, Genomes, Genetics. doi: 10.1534/g3.119.400346

Moreira FF, Oliveira HR, Volenec JJ, Rainey KM, Brito LF (2020) Integrating High-Throughput Phenotyping and Statistical Genomic Methods to Genetically Improve Longitudinal Traits in Crops. Frontiers in Plant Science. doi: 10.3389/fpls.2020.00681

Moriana A, Villalobos FJ, Fereres E (2002) Stomatal and photosynthetic responses of olive (Olea europaea L.) leaves to water deficits. Plant, Cell and Environment **25**: 395–405

873 **Moshelion M** (2020a) The dichotomy of yield and draught resistance. EMBO reports
874 1–7

875 **Moshelion M** (2020b) The dichotomy of yield and drought resistance. EMBO reports
876 **21**: 1–7

877 **Moshelion M, Altman A** (2015) Current challenges and future perspectives of plant
878 and agricultural biotechnology. Trends in Biotechnology **33**: 337–342

879 **Muir CD, Pease JB, Moyle LC** (2014) Quantitative genetic analysis indicates natural
880 selection on leaf phenotypes across wild tomato species (Solanum sect.
881 lycopersicon; solanaceae). Genetics **198**: 1629–1643

882 **Negin B, Moshelion M** (2017) The advantages of functional phenotyping in pre-field
883 screening for drought-tolerant crops. Functional Plant Biology **44**: 107

884 **Ohsumi A, Kanemura T, Homma K, Horie T, Shiraiwa T** (2007) Genotypic variation of
885 stomatal conductance in relation to stomatal density and length in rice (Oryza
886 sativa L.). Plant Production Science. doi: 10.1626/pps.10.322

887 **Paradiso R, de Visser PHB, Arena C, Marcelis LFM** (2020) Light response of
888 photosynthesis and stomatal conductance of rose leaves in the canopy profile:
889 the effect of lighting on the adaxial and the abaxial sides. Functional plant
890 biology : FPB. doi: 10.1071/FP19352

891 **Resco de Dios V, Loik ME, Smith R, Aspinwall MJ, Tissue DT** (2016) Genetic variation
892 in circadian regulation of nocturnal stomatal conductance enhances carbon
893 assimilation and growth. Plant Cell and Environment **39**: 3–11

894 **Sakoda K, Yamori W, Shimada T, Sugano SS, Hara-Nishimura I, Tanaka Y** (2020a)
895 Stomatal density affects gas diffusion and CO2 assimilation dynamics in
896 Arabidopsis under fluctuating light. bioRxiv. doi: 10.1101/2020.02.20.958603

897 **Sakoda K, Yamori W, Shimada T, Sugano SS, Hara-Nishimura I, Tanaka Y** (2020b)
898 Higher Stomatal Density Improves Photosynthetic Induction and Biomass
899 Production in Arabidopsis Under Fluctuating Light. Frontiers in Plant Science.
900 doi: 10.3389/fpls.2020.589603

901 **Sallam A, Alqudah AM, Dawood MFA, Baenziger PS, Börner A** (2019) Drought stress
902 tolerance in wheat and barley: Advances in physiology, breeding and genetics
903 research. International Journal of Molecular Sciences. doi:
904 10.3390/ijms20133137

905 **Sandhu KS, Mihalyov PD, Lewien MJ, Pumphrey MO, Carter AH** (2021) Combining
906 Genomic and Phenomic Information for Predicting Grain Protein Content and
907 Grain Yield in Spring Wheat. Frontiers in Plant Science. doi:
908 10.3389/fpls.2021.613300

909 **Schlichting C** (1986) The Evolution of Phenotypic Plasticity in Plants. Annual Review
910 of Ecology and Systematics. doi: 10.1146/annurev.ecolsys.17.1.667

911 **Schoppach R, Sinclair TR, Sadok W** (2020) Sleep tight and wake-up early: Nocturnal
912 transpiration traits to increase wheat drought tolerance in a Mediterranean
913 environment. Functional Plant Biology. doi: 10.1071/FP20044

914 **Shahinnia F, Roy J le, Laborde B, Sznajder B, Kalambettu P, Mahjourimajd S,**
915 **Tilbrook J, Fleury D** (2016) Genetic association of stomatal traits and yield in

wheat grown in low rainfall environments. BMC Plant Biology. doi: 10.1186/s12870-016-0838-9

Sinclair TR (2011) Challenges in breeding for yield increase for drought. Trends in Plant Science **16**: 289–293

Sinclair TR (2018) Effective water use required for improving crop growth rather than transpiration efficiency. Frontiers in Plant Science **9**: 1–8

Snowdon RJ, Wittkop B, Chen TW, Stahl A (2020) Crop adaptation to climate change as a consequence of long-term breeding. Theoretical and Applied Genetics **134**: 1613–1623

Sultana SN, Park H, Choi SH, Jo H, Song JT, Lee J-D, Kang YJ (2021) Optimizing the Experimental Method for Stomata-Profiling Automation of Soybean Leaves Based on Deep Learning. Plants **10**: 2714

Tatsumi K, Kuwabara Y, Motobayashi T (2020) Photosynthetic light-use efficiency of rice leaves under fluctuating incident light. Agrosystems, Geosciences and Environment. doi: 10.1002/agg2.20030

TEARE ID, KANEMASU ET (1972) STOMATAL-DIFFUSION RESISTANCE AND WATER POTENTIAL OF SOYBEAN AND SORGHUM LEAVES. New Phytologist. doi: 10.1111/j.1469-8137.1972.tb01959.x

Thao NP, Tran L-SP (2016) Enhancement of Plant Productivity in the Post-Genomics Era. Current genomics **17**: 295–6

936 **Tian Z, Wang JW, Li J, Han B** (2021) Designing future crops: challenges and strategies
937 for sustainable agriculture. Plant Journal. doi: 10.1111/tpj.15107

938 **TURNER NC** (1970) RESPONSE OF ADAXIAL AND ABAXIAL STOMATA TO LIGHT. New
939 Phytologist. doi: 10.1111/j.1469-8137.1970.tb02452.x

940 **Ullmann I, Lange OL, Ziegler H, Ehleringer J, Schulze ED, Cowan IR** (1985) Diurnal
941 courses of leaf conductance and transpiration of mistletoes and their hosts in
942 Central Australia. Oecologia **67**: 577–587

943 **Voss-Fels KP, Cooper M, Hayes BJ** (2019) Accelerating crop genetic gains with
944 genomic selection. Theoretical and Applied Genetics. doi: 10.1007/s00122-018-
945 3270-8

946 **Walpita P, Flick R** (2005) Reverse genetics of negative-stranded RNA viruses: A global
947 perspective. FEMS Microbiology Letters. doi: 10.1016/j.femsle.2005.01.046

948 **Wang Y, Noguchi K, Terashima I** (2008) Distinct light responses of the adaxial and
949 abaxial stomata in intact leaves of Helianthus annuus L. Plant, Cell and
950 Environment. doi: 10.1111/j.1365-3040.2008.01843.x

951 **Wardle GM** (2013) Pillars of Evolution. Fundamental Principles of the Eco-
952 evolutionary Process by Douglas W. Morris & Per Lundberg. Oxford University
953 Press, New York, 2011. viii + 272 pp. Price AUD $62.95 (paperback). ISBN 978-0-
954 19-856880-3. Austral Ecology. doi: 10.1111/aec.12092

955 **Yang R, Tian Q, Xu S** (2006) Mapping quantitative trait loci for longitudinal traits in
956 line crosses. Genetics. doi: 10.1534/genetics.105.054775

957 **Zhang ZS, Li YT, Gao HY, Yang C, Meng QW** (2016) Characterization of

958 photosynthetic gas exchange in leaves under simulated adaxial and abaxial

959 surfaces alternant irradiation. Scientific Reports. doi: 10.1038/srep26963

960

961

Figure 1

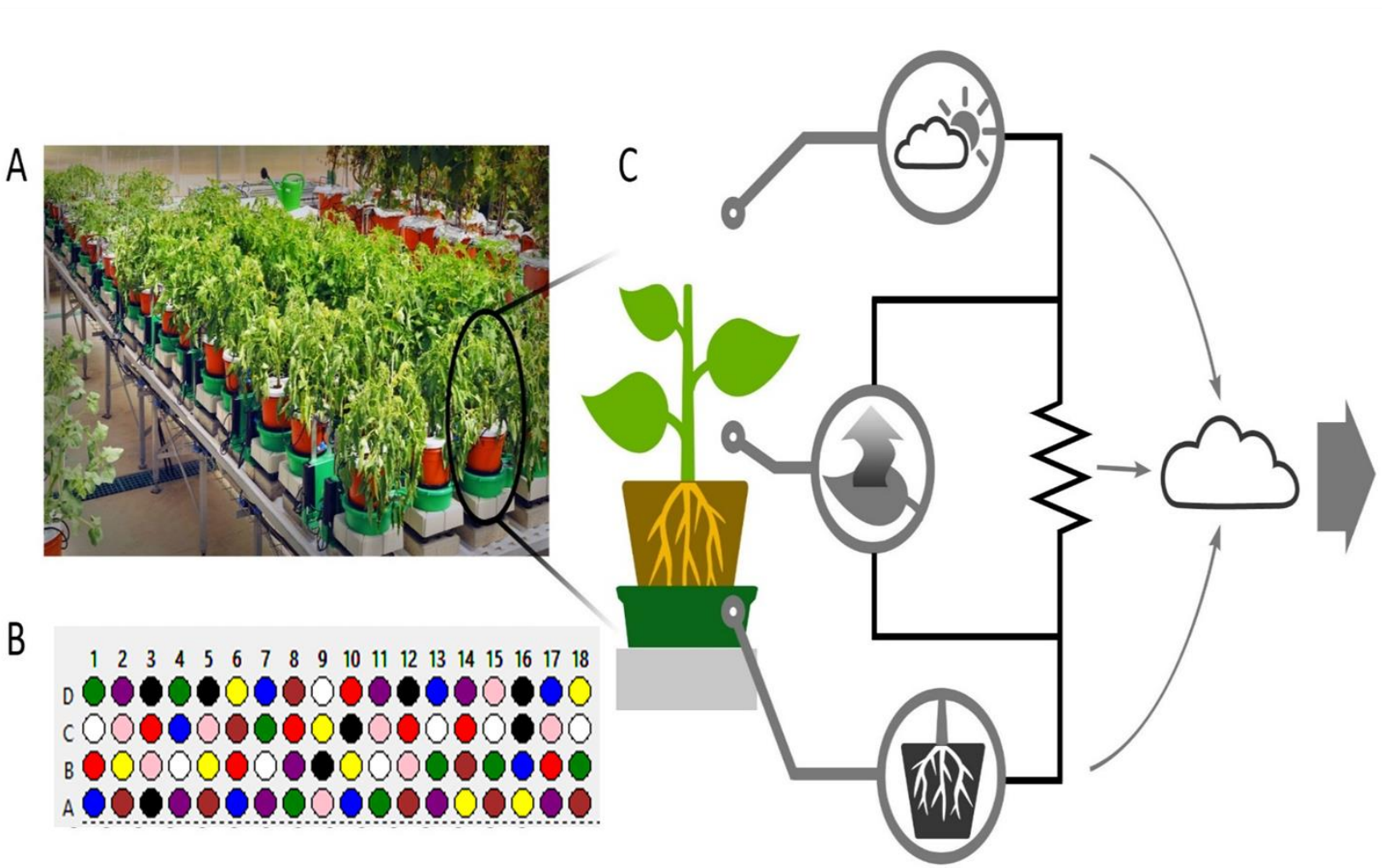

Gosa et al.,2022

Figure 2

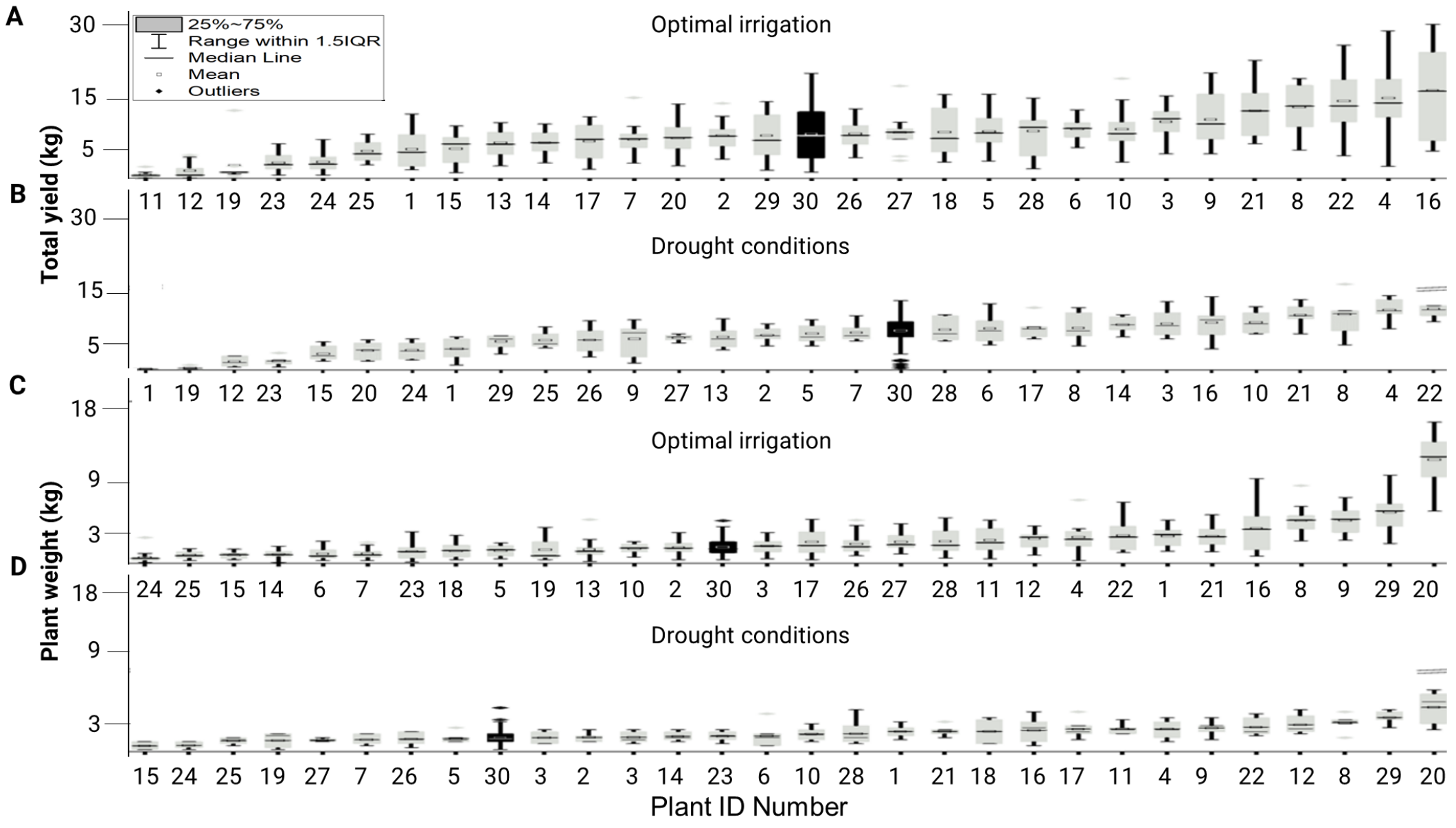

Code	LINE
1	IL10-1
2	IL10-2
3	IL11-4
4	IL12-1-1
5	IL12-2
6	IL12-3-1
7	IL2-1-1
8	IL2-4
9	IL2-6
10	IL2-6-5
11	IL3-3
12	IL3-4
13	IL4-1
14	IL4-1-1
15	IL4-3-2
16	IL5-2
17	IL5-3
18	IL5-5
19	IL6-2
20	IL6-3
21	IL6-4
22	IL7-4-1
23	IL8-1
24	IL8-1-1
25	IL8-1-3
26	IL9-1
27	IL9-1-3
28	IL9-2-6
29	IL9-3
30	M82

Gosa et al.,2022

Table 1

		Well irrigation treatment		Drought treatment					
line	ID Number	Fruit yield	Shoot weight	Fruit yield	Shoot weight	Group classification	Abbreviation	Classification Number	
M82	30	CONTROL	CONTROL	CONTROL	CONTROL	Control			*
IL12-1-1	4	HIGH	HIGH	HIGH	HIGH	High yielder High biomass High tolerance High resilience - IDEOTYPE	HyHbHtHr	1	
IL5-2	16	HIGH	HIGH	HIGH	HIGH	High yielder High biomass High tolerance High resilience - IDEOTYPE	HyHbHtHr	1	*
IL6-4	26	HIGH	HIGH	HIGH	HIGH	High yielder High biomass High tolerance High resilience - IDEOTYPE	HyHbHtHr	1	
IL7-4-1	22	HIGH	HIGH	HIGH	HIGH	High yielder High biomass High tolerance High resilience - IDEOTYPE	HyHbHtHr	1	
IL2-4	8	HIGH	HIGH	MEDIUM	HIGH	High yielder High biomass Medium tolerance High resilience	HyHbMtHr	2	
IL2-6	9	HIGH	HIGH	LOW	HIGH	High yielder High biomass Low tolerance High resilience	HyHbLtHr	3	*
IL11-4	3	HIGH	MEDIUM	MEDIUM	MEDIUM	High yielder Medium biomass Medium tolerance Medium resilience	HyMbMtMr	4	*
IL6-3	20	MEDIUM	HIGH	LOW	HIGH	Medium yielder High biomass Low tolerance High resilience	MyHbLtHr	5	
IL9-3	29	MEDIUM	HIGH	LOW	HIGH	Medium yielder High biomass Low tolerance High resilience	MyHbLtHr	5	
IL9-1	26	MEDIUM	HIGH	LOW	MEDIUM	Medium yielder High biomass Low tolerance Medium resilience	MyHbLtMr	6	
IL9-2-6	28	MEDIUM	HIGH	MEDIUM	HIGH	Medium yielder High biomass Medium tolerance High resilience	MyHbMtHr	7	
IL2-6-5	10	MEDIUM	MEDIUM	HIGH	HIGH	Medium yielder Medium biomass High tolerance High resilience	MyMbHtHr	8	
IL5-3	17	MEDIUM	MEDIUM	MEDIUM	HIGH	Medium yielder Medium biomass Medium tolerance High resilience	MyMbMtHr	9	
IL9-1-3	27	MEDIUM	MEDIUM	MEDIUM	LOW	Medium yielder Medium biomass Medium tolerance Low resilience	MyMbMtLr	10	
IL10-2	2	MEDIUM	MEDIUM	MEDIUM	MEDIUM	Medium yielder Medium biomass Medium tolerance Medium resilience	MyMbMtMr	11	
IL5-5	18	MEDIUM	SMALL	HIGH	HIGH	Medium yielder Small biomass High tolerance High resilience	MySbHtHr	12	
IL2-1-1	7	MEDIUM	SMALL	MEDIUM	LOW	Medium yielder Small biomass Medium tolerance Low resilience	MySbMtLr	13	
IL12-2	5	MEDIUM	SMALL	MEDIUM	MEDIUM	Medium yielder Small biomass Medium tolerance Medium resilience	MySbMtMr	14	
IL12-3-1	6	MEDIUM	SMALL	MEDIUM	MEDIUM	Medium yielder Small biomass Medium tolerance Medium resilience	MySbMtMr	14	
IL10-1	1	LOW	HIGH	LOW	HIGH	Low yielder High biomass Low tolerance High resilience	LyHbLtHr	15	*
IL3-3	11	LOW	HIGH	LOW	HIGH	Low yielder High biomass Low tolerance High resilience	LyHbLtHr	15	
IL3-4	12	LOW	HIGH	LOW	HIGH	Low yielder High biomass Low tolerance High resilience	LyHbLtHr	15	
IL6-2	19	LOW	MEDIUM	LOW	LOW	Low yielder Medium biomass Low tolerance Low resilience	LyMbLtLr	16	
IL4-1	13	LOW	MEDIUM	MEDIUM	MEDIUM	Low yielder Medium biomass Medium tolerance Medium resilience	LyMbMtMr	17	
IL4-1-1	14	LOW	SMALL	MEDIUM	MEDIUM	Low yielder Small biomass Medium tolerance Medium resilience	LySbMtMr	18	
IL8-1	23	LOW	SMALL	LOW	MEDIUM	Low yielder Small biomass Low tolerance Medium resilience	LySbLtMr	19	*
IL8-1-3	25	LOW	SMALL	LOW	LOW	Low yielder Small biomass Low tolerance Low resilience- SURVIVAL	LySbLtLr	20	*
IL4-3-2	15	LOW	SMALL	LOW	LOW	Low yielder Small biomass Low tolerance Low resilience - SURVIVAL	LySbLtLr	20	
IL8-1-1	24	LOW	SMALL	LOW	LOW	Low yielder Small biomass Low tolerance Low resilience- SURVIVAL	LySbLtLr	20	

Figure 3

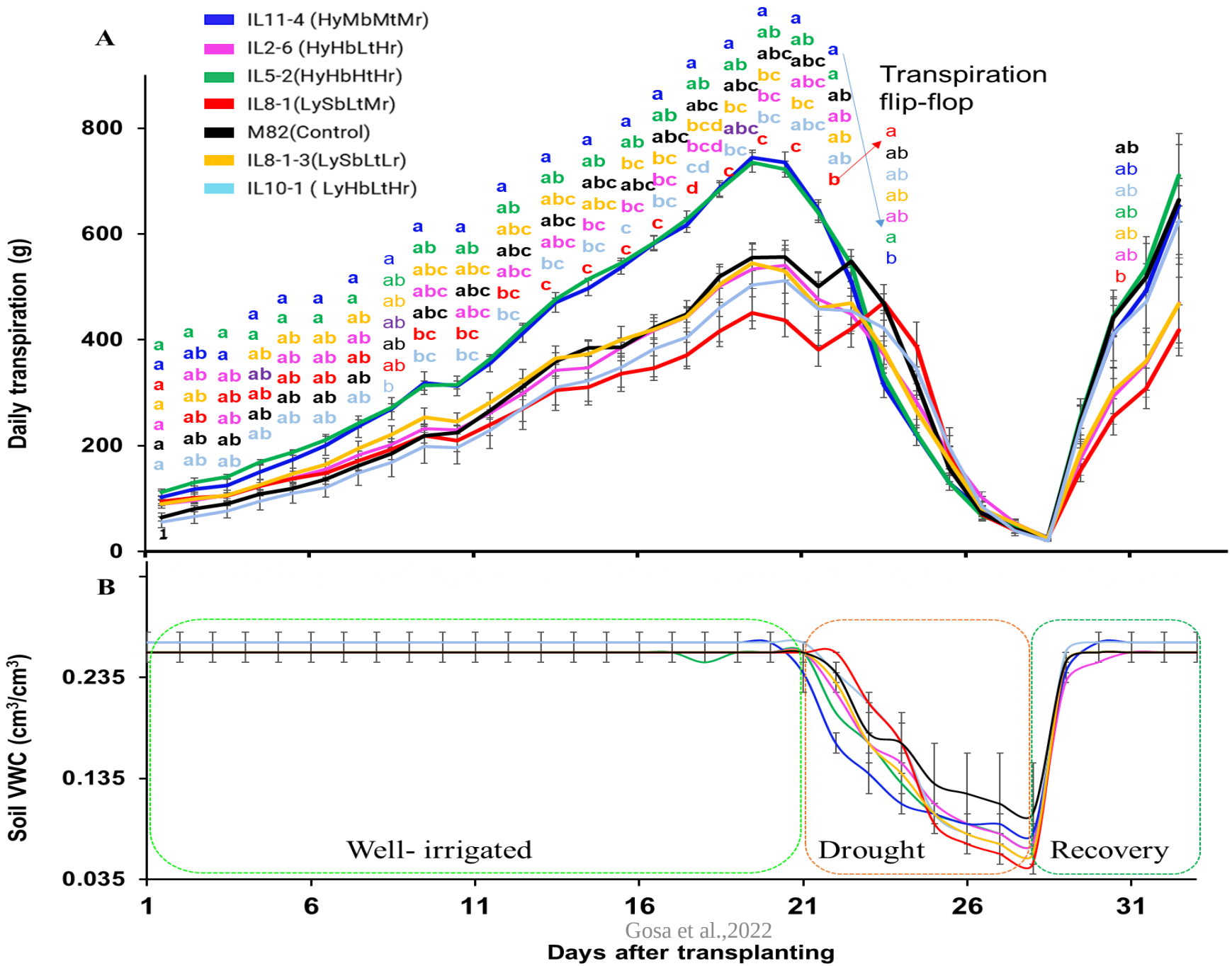

Gosa et al.,2022

Figure 4

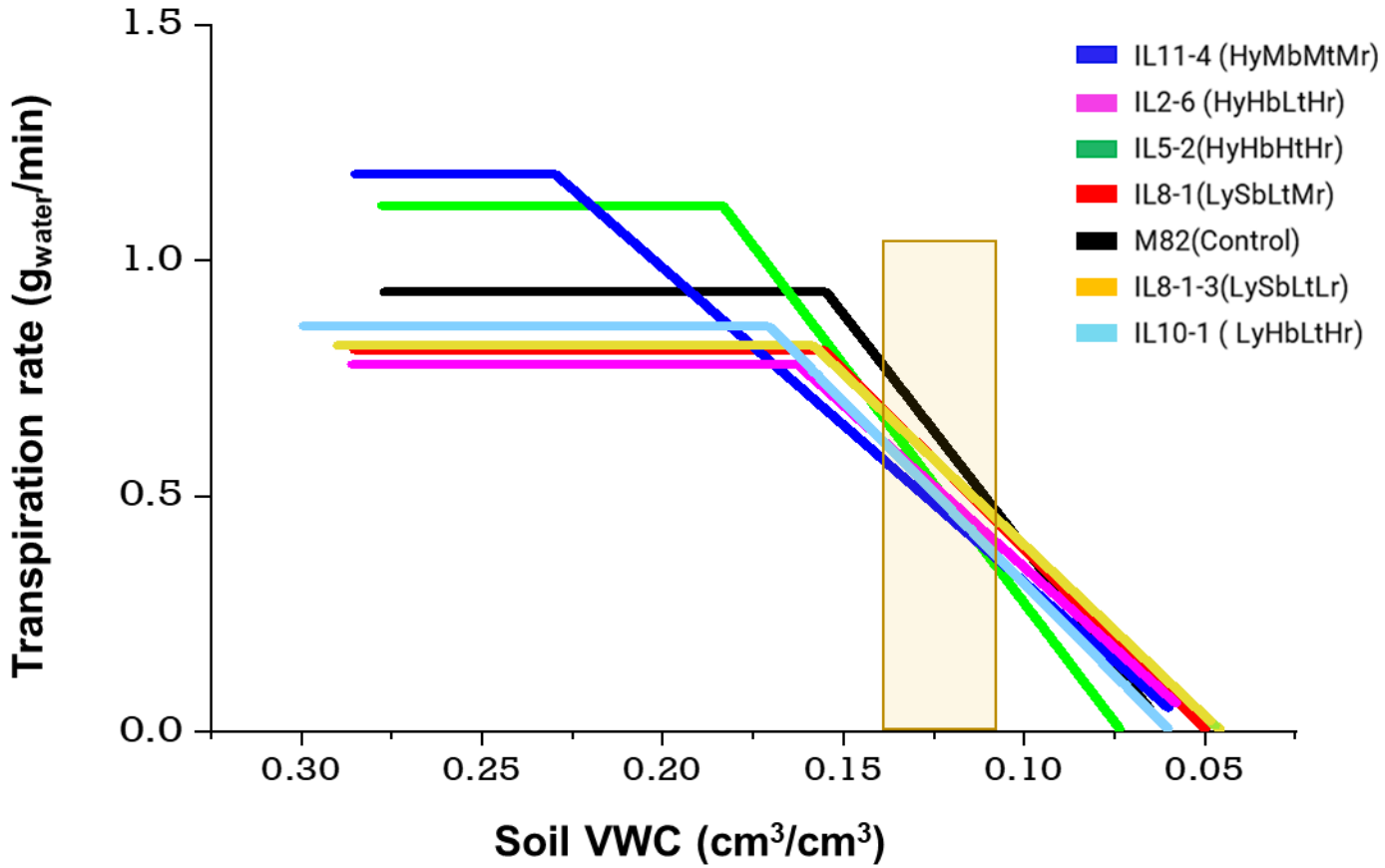

Gosa et al.,2022

Figure 5

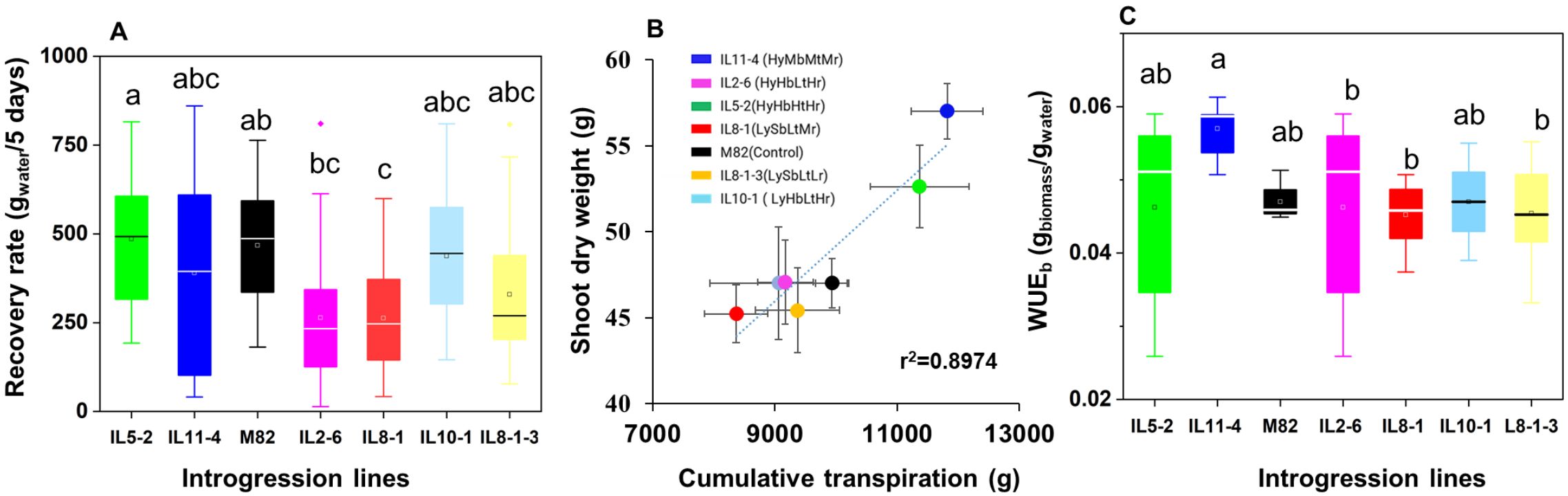
A
Recovery rate (g_{water}/5 days)
1000
750
500
250
0
a
abc
ab
bc
c
abc
abc
IL5-2
IL11-4
M82
IL2-6
IL8-1
IL10-1
IL8-1-3
Introgression lines
B
Shoot dry weight (g)
60
55
50
45
40
IL11-4 (HyMbMtMr)
IL2-6 (HyHbLtHr)
IL5-2(HyHbHtHr)
IL8-1(LySbLtMr)
M82(Control)
IL8-1-3(LySbLtLr)
IL10-1 (LyHbLtHr)
r^2=0.8974
7000
9000
11000
13000
Cumulative transpiration (g)
C
WUE_b ($g_{biomass}$/g_{water})
0.06
0.04
0.02
ab
a
ab
b
b
ab
b
IL5-2
IL11-4
M82
IL2-6
IL8-1
IL10-1
L8-1-3
Introgression lines

Figure 6

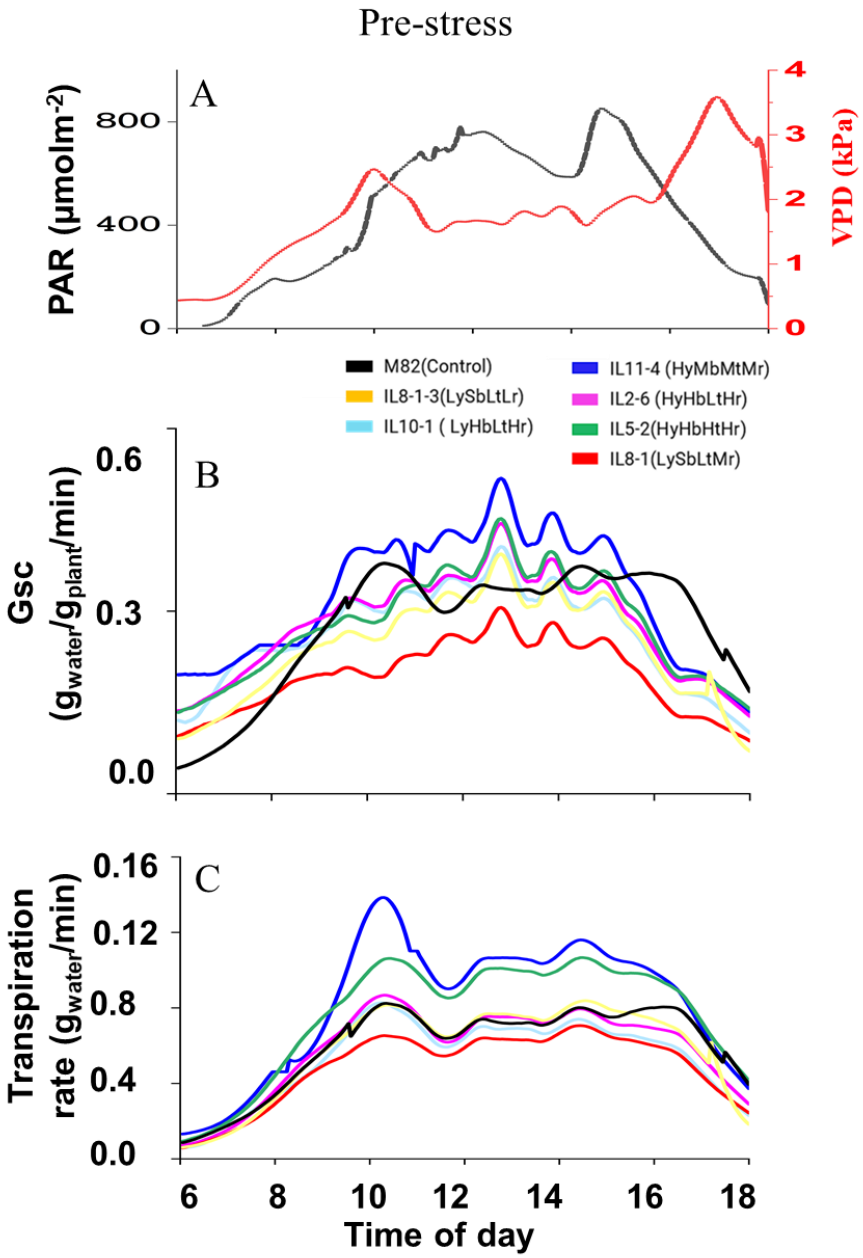

Gosa et al.,2022

Figure 8

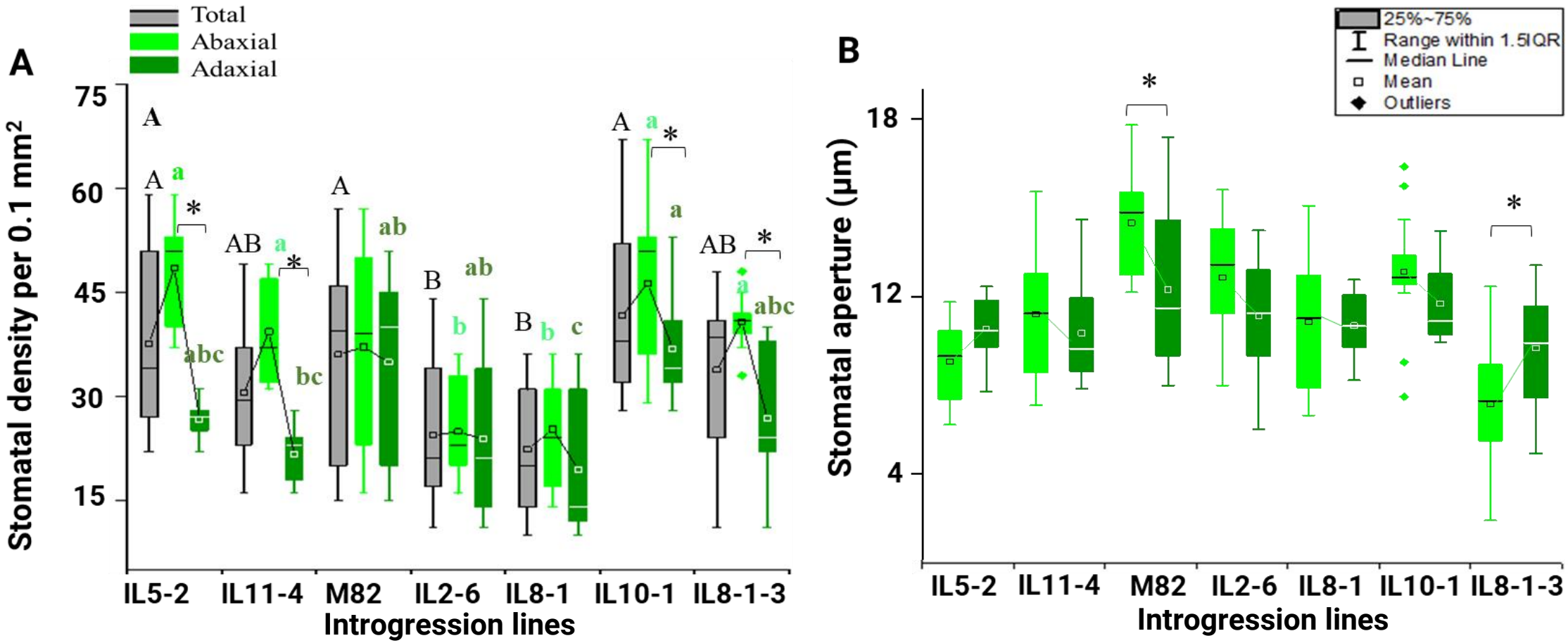
A
Total
Abaxial
Adaxial
Stomatal density per 0.1 mm²
75
60
45
30
15
A
A a *
abc
AB a *
bc
A
ab
B
ab
b
B b c
A a *
a
AB *
a
abc
IL5-2
IL11-4
M82
IL2-6
IL8-1
IL10-1
IL8-1-3
Introgression lines
B
25%~75%
Range within 1.5IQR
Median Line
Mean
Outliers
Stomatal aperture (μm)
18
12
4
*
*
IL5-2
IL11-4
M82
IL2-6
IL8-1
IL10-1
IL8-1-3
Introgression lines

Figure 10

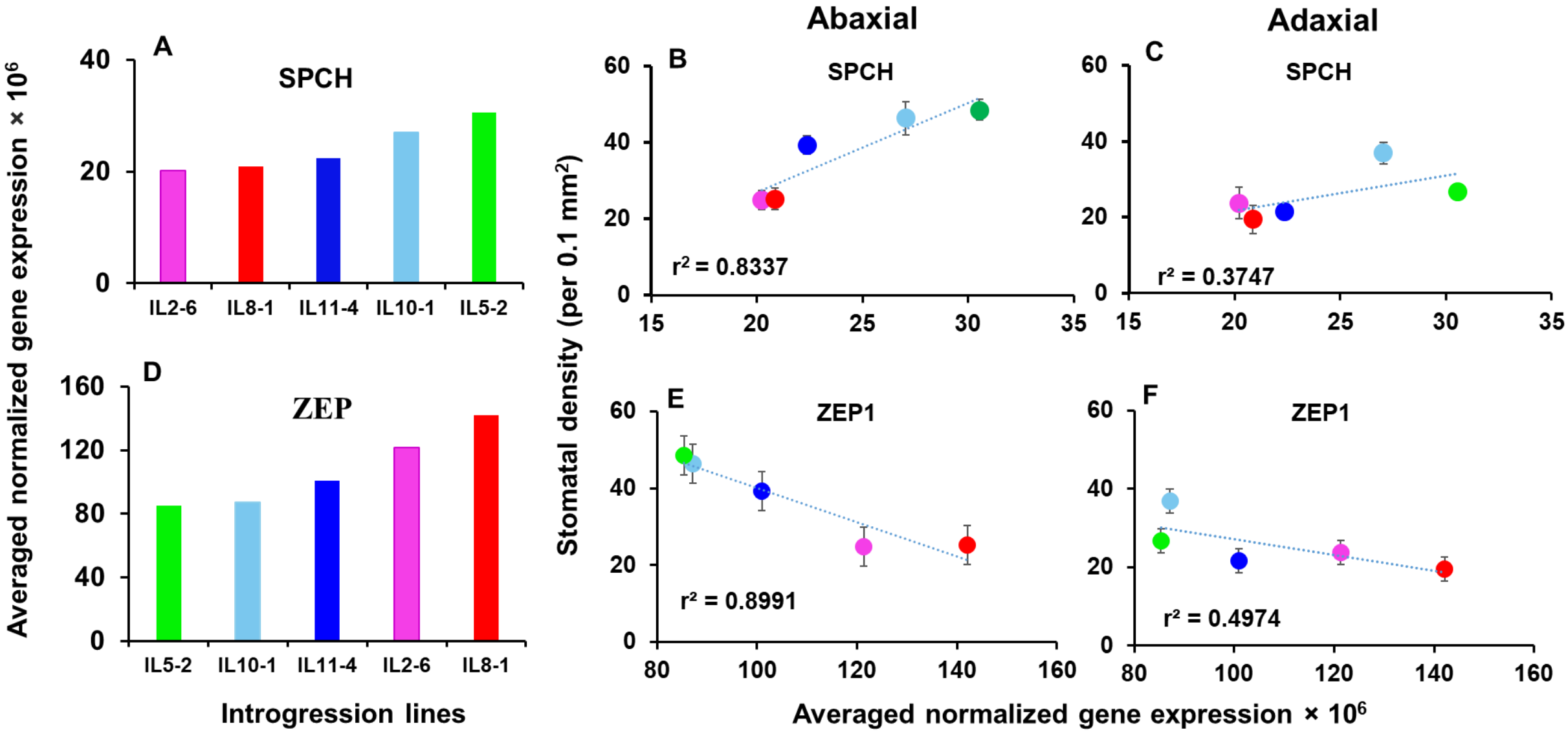
A
SPCH
Averaged normalized gene expression × 10⁶
40
20
0
IL2-6
IL8-1
IL11-4
IL10-1
IL5-2
D
ZEP
160
120
80
40
0
IL5-2
IL10-1
IL11-4
IL2-6
IL8-1
Introgression lines
Abaxial
Adaxial
B
SPCH
r² = 0.8337
C
SPCH
r² = 0.3747
E
ZEP1
r² = 0.8991
F
ZEP1
r² = 0.4974
Stomatal density (per 0.1 mm²)
60
40
20
0
15
20
25
30
35
80
100
120
140
160
Averaged normalized gene expression × 10⁶

Supplementary

Supplementary Figure 1

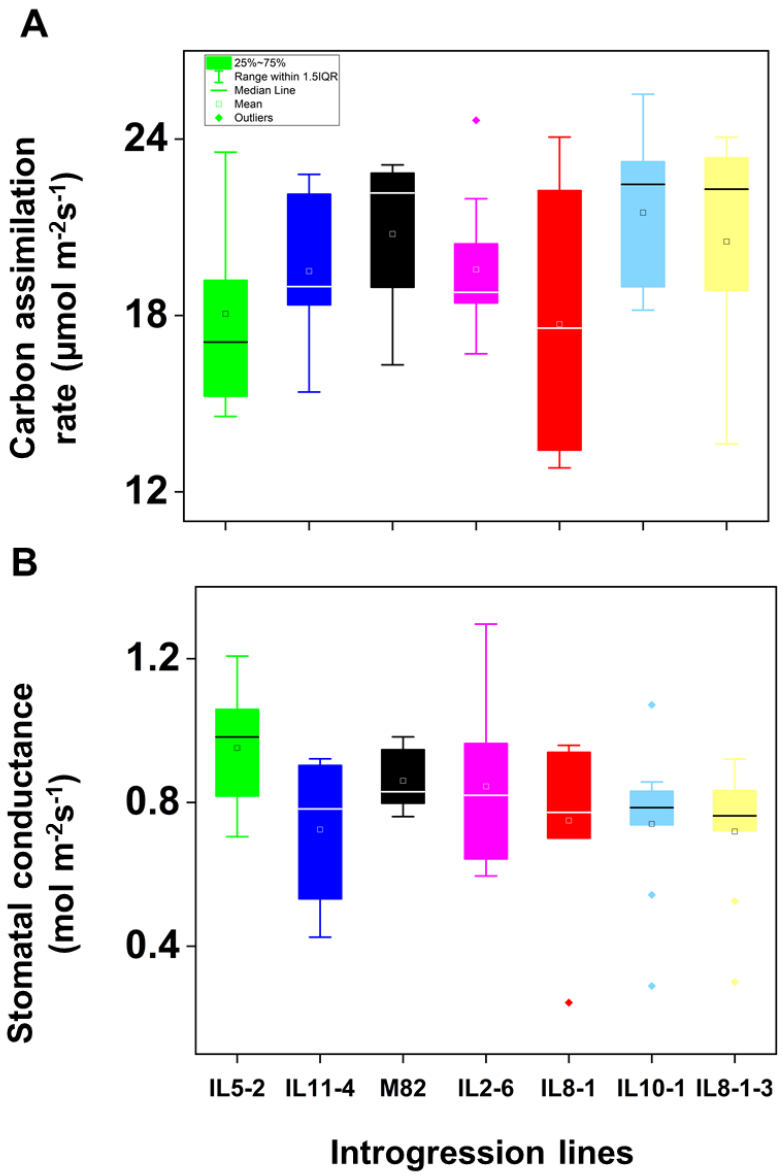

Gosa et al.,2022

Supplementary Figure 2

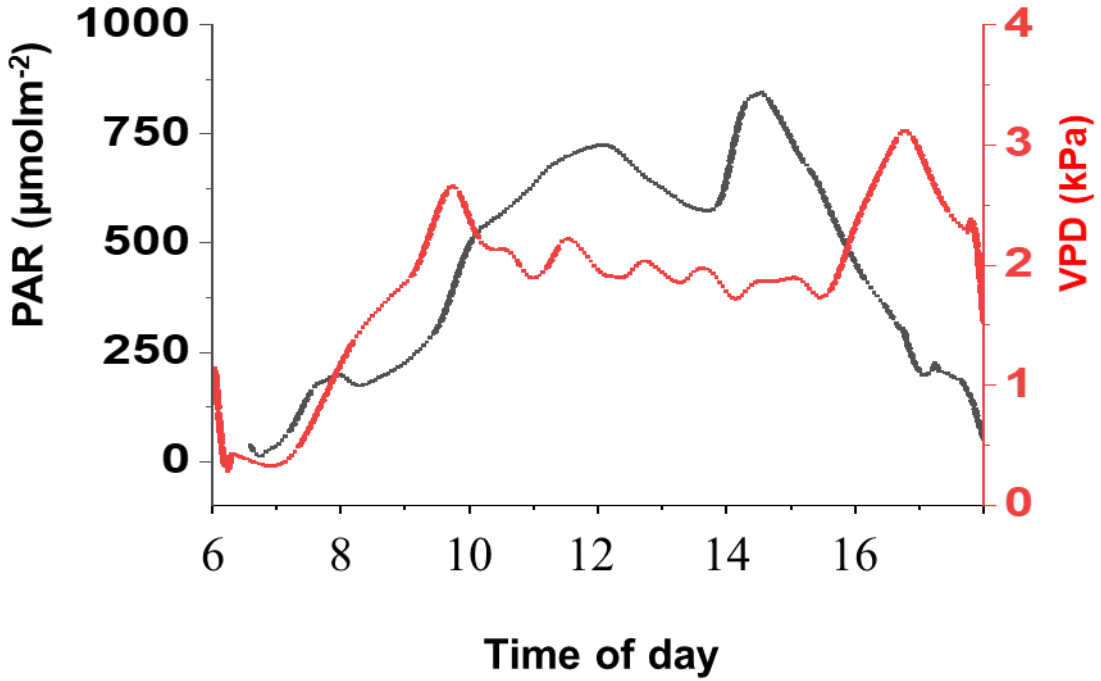

Figure 7

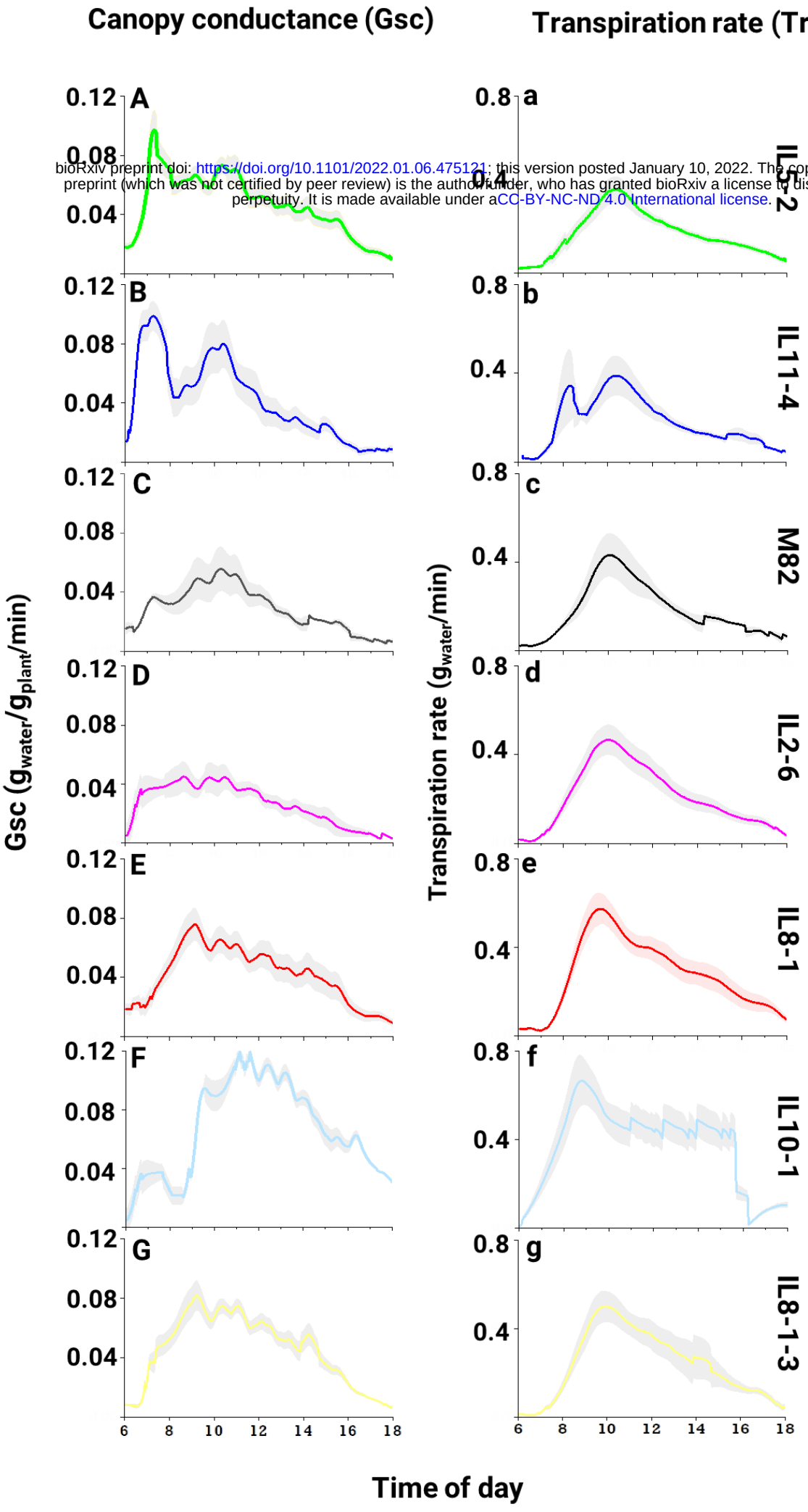

Figure 9